
ERROR FEEDBACK CAN ACCURATELY COMPRESS PRECONDITIONERS

Ionut-Vlad Modoranu*

IST Austria

ionut-vlad.modoranu@ist.ac.at

Aleksei Kalinov

IST Austria

aleksei.kalinov@ist.ac.at

Eldar Kurtic

IST Austria

eldar.kurtic@ist.ac.at

Dan Alistarh

IST Austria

dan.alistarh@ist.ac.at

ABSTRACT

Leveraging second-order information at the scale of deep networks is one of the main lines of approach for improving the performance of current optimizers for deep learning. Yet, existing approaches for accurate full-matrix preconditioning, such as Full-Matrix Adagrad (GGT) or Matrix-Free Approximate Curvature (M-FAC) suffer from massive storage costs when applied even to medium-scale models, as they must store a sliding window of gradients, whose memory requirements are multiplicative in the model dimension. In this paper, we address this issue via an efficient and simple-to-implement error-feedback technique that can be applied to compress preconditioners by up to two orders of magnitude in practice, without loss of convergence. Specifically, our approach compresses the gradient information via sparsification or low-rank compression *before* it is fed into the preconditioner, feeding the compression error back into future iterations. Extensive experiments on deep neural networks for vision show that this approach can compress full-matrix preconditioners by up to two orders of magnitude without impact on accuracy, effectively removing the memory overhead of full-matrix preconditioning for implementations of full-matrix Adagrad (GGT) and natural gradient (M-FAC). Our code is available at <https://github.com/IST-DASLab/EFCP>.

1 Introduction

The remarkable success of stochastic gradient descent (SGD)-based optimizers in deep learning motivated a long line of research for accelerated variants that would scale to the massive parameter and dataset sizes common in the area. Among these, optimizers based on adaptive regularization, such as Adagrad [10] and Adam [18] are extremely well-established results, with myriads of extensions, e.g. [2, 1, 42, 15]. While very successful, most practical approaches restrict the preconditioning of the descent direction to correspond to a diagonal matrix. By contrast, a very promising but less developed direction employs what we call *full-matrix preconditioning*, pre-multiplying the descent direction with a full matrix, whose structure is justified either via adaptive regularization [1], or via approximations of natural gradient such as the Fisher approximation [5, 12].

Yet, existing implementations of full-matrix preconditioning are currently impractical given their significant memory costs. Specifically, both full-matrix adaptive preconditioning methods such as GGT [1] and full-matrix natural-gradient inspired methods such as M-FAC [12] require maintaining a “sliding window” of past gradients, which are employed in estimating the preconditioner at each step. Even for medium-sized models, maintaining the gradient history results in unmanageable total cost of $\Theta(md)$ memory, where d is the model dimension, usually in the millions, and m is the size of the gradient history, usually of size 100-1000. For example, training the standard ResNet-18 computer vision model on ImageNet using M-FAC via a standard recipe would require 56GB of GPU RAM, which is unavailable on most existing GPUs. Thus, while showing promising results, full-matrix preconditioning is currently impractical at scale due to memory constraints.

*Corresponding author.

Contribution. In this paper, we propose a solution to this issue, in the form of an approach called Compressed Preconditioning with Error Feedback (EFCP), which can be applied to both adaptive (Adagrad/GGT) and natural-gradient (M-FAC) full-matrix preconditioners. EFCP can apply either sparse or low-rank compression of the gradient history matrix; for both compression variants, we provide efficient compression-aware implementations which can leverage compression for significant memory savings. On the practical side, we show that compressed sparse preconditioners can be maintained efficiently on GPUs, and provide experimental evidence that EFCP can compress the gradient history by up to two orders of magnitude without affecting end accuracy, relative to uncompressed full-matrix preconditioning. For example, EFCP applied to the M-FAC optimizer can outperform the Top-1 accuracy of tuned SGD [22] for the ResNet18 model on ImageNet, while using $\leq 10\%$ more peak memory than vanilla SGD.

In more detail, EFCP works as follows. Consider a full-matrix preconditioner algorithm, such as GGT or M-FAC: these algorithms maintain a sliding window of the m past SGD gradients, each of dimension d , which are used to generate an estimate of the full-matrix preconditioner at the current optimization step. The key idea behind EFCP is that we only wish to maintain a history of *compressed gradients* for the preconditioning. However, naive direct compression, e.g. via truncation or stochastic rounding leads to divergence. Instead, we show that we can compress the entire gradient history without impacting the preconditioner significantly if we feed back the compression error from previous iterations into the gradient estimate at each step, before it enters the preconditioner, a process known as error feedback, e.g. [17].

With this in place, we show that EFCP is compatible both with sparsification (Top- k) and with low-rank gradient compression, both of which can significantly reduce memory cost. In both cases, we provide new algorithms for efficiently updating the preconditioner data-structure under compressed updates, which realize the memory savings efficiently in practice.

On the experimental side, we implement EFCP efficiently in the context of some of the best currently-known full-matrix preconditioners, GGT and M-FAC. We examine its performance on a standard convex problem, on computer vision tasks, i.e. training residual networks (ResNets) on CIFAR [20] and ImageNet [33], as well as BERT models [8] on common language modelling tasks [39]. The experiments show that, across all tasks, individual gradients stored in the history can be compressed extremely significantly: for instance, we can prune gradients to $\geq 99\%$ sparsity without loss of convergence or validation accuracy, relative to uncompressed preconditioning.

2 Background and Related Work

2.1 General Setting

We consider a standard classification setting, in which we are given a training dataset $\mathcal{D} = \{(x_i, y_i)_{i=1}^N\}$ containing N i.i.d. samples x_i and their associated labels y_i . We suppose input pairs (x, y) are drawn from a true, unknown distribution $p_{true} \triangleq p_t$ having the density $p_t(x, y) = p_t(x)p_t(y|x)$ and our model $\theta \in \mathbb{R}^d$ parameterizes a probabilistic distribution $p_\theta(y|x) \triangleq p(y|f(x, \theta))$ with density $p_\theta(x, y) = p_t(x)p_\theta(y|x)$. Our aim is to minimize the ‘‘difference’’ between the true conditional distribution $p_t(y|x)$ and the modelled conditional distribution $p_\theta(y|x)$, measured in some appropriate metric. If we pick this to be the KL divergence between the two distributions, we obtain:

$$KL(p_t(x, y)||p_\theta(x, y)) = \int p_t(x, y) \log \frac{p_t(x, y)}{p_\theta(x, y)} dx dy = \mathbb{E}_{p_t(x)}[KL(p_t(y|x)||p_\theta(y|x))]. \quad (1)$$

In practice, we only have a finite number of samples $x \sim p_t(x)$ and no information about the density function. In this case, we are using the empirical training distribution \hat{p}_t instead of p_t , which is given by the samples in \mathcal{D} and thus we can define the loss as

$$L(\theta) \triangleq KL(p_t(x, y)||p_\theta(x, y)) = \mathbb{E}_{\hat{p}_t(x)}[KL(p_t(y|x)||p_\theta(y|x))] \approx -\frac{1}{N} \sum_{i=1}^N \log p_\theta(y_i|x_i). \quad (2)$$

which is the standard objective function minimized for the maximum likelihood estimation. It is common to assume that the loss $L : \mathbb{R}^d \rightarrow \mathbb{R}$ is continuous and twice differentiable.

In practice, the loss L in Equation 2 is often minimized using variants of Stochastic Gradient Descent (SGD) $\theta_{t+1} \leftarrow \theta_t - \eta_t g_t$, where $g_t \triangleq \nabla_\theta L(\theta_t)$ and $\eta_t \in \mathbb{R}$ is the learning rate. However, theoretical results suggest that convergence and end-results can be improved by *preconditioning* this gradient with a matrix C which incorporates information about the geometry of the loss landscape, leading to the parameter update rule

$$\theta_{t+1} \leftarrow \theta_t - \eta_t C_t^{-1} g_t. \quad (3)$$

Natural Gradient. A popular approach for estimating a good preconditioner is Natural Gradient [4], which adapts to the information geometry of the loss landscape by measuring the discrepancy between the true distribution and

the modelled distribution in terms of KL-divergence in the distribution space, as opposed to using the Euclidean distance as is the case for regular SGD. Then, the preconditioner C is the Fisher Information Matrix (FIM), defined as $F(\theta) \triangleq \frac{1}{N} \sum_{i=1}^N \mathbb{E}_{p_\theta(y|x_i)} [\nabla_\theta \log p_\theta(y|x_i) \nabla_\theta \log p_\theta(y|x_i)^T]$. In this context, one can show that the FIM is the expected Hessian with respect to the log-likelihood. Since the exact FIM is difficult to compute due to the expectation term in its definition, different efficient approximations of it exist in the literature. For neural networks, K-FAC [14, 27] provides a diagonal and tri-diagonal approximation of FIM by sampling a limited number of y values from $p_\theta(y|x_i)$ in order to compute the expectation.

Another popular approximation to the FIM is the Empirical Fisher, defined as $\hat{F}(\theta) \triangleq \frac{1}{N} \sum_{i=1}^N \nabla_\theta \log p_\theta(y_i|x_i) \nabla_\theta \log p_\theta(y_i|x_i)^T$. Instead of sample y 's from model's predictive distribution, it uses the associated label y_i . It is important to note that the empirical Fisher is a good approximation of the FIM if $p_t(y|x) \approx p_\theta(y|x)$, e.g. when the model has good accuracy. The M-FAC method [12] (Section 2.2) provides an efficient implementation for this approach.

Adaptive Regularization. A different justification for obtaining good preconditioners is via *adaptive regularization*, arising from online convex optimization. Broadly, the idea is to adapt the learning rate corresponding to each parameter in order to minimize regret, defined as the cumulative difference between the optimizer's performance and the best decision in hindsight, by taking into account the history of gradients observed up to a given point. By and large, the community has focused on diagonal preconditioners, which allow computationally-efficient and extremely popular algorithms, such as Adam [18] and AdaGrad [10]. The GGT result [1] (Section 2.2) showed that results can be improved by taking "second-order" weight correlations into account, leading to a full-matrix, $d \times d$ preconditioner, and provided an efficient approximation of this preconditioner.

2.2 Efficient Preconditioners and Related Methods

Overview. We now provide a detailed description of the GGT [1] and M-FAC [12] approaches, which will later serve as the main illustrations of our preconditioner compression method. A key common point of both methods is the fact that they store a history of the past m gradients in the matrix

$$G = [g_{t-m+1}^T, g_{t-m+2}^T, \dots, g_{t-1}^T, g_t^T] \in \mathbb{R}^{m \times d},$$

which is represented as a ring buffer, updated at each step by replacing the oldest gradient g_{t-m+1} with the most recently-generated one g_t . The *difference* in methods comes from the way the ring buffer G_t is used to approximate the preconditioner. To preserve performance the buffer G_t must be stored in the GPU memory. For best accuracy both methods require between 100 and 1000 gradients to be stored, each of which of size d (the model dimension), thus, the memory cost of each method becomes intractable. Next, we briefly describe the algorithmic implementation of these methods.

The M-FAC method provides an efficient estimator for Inverse-Hessian-Vector-Products (IHVP) for the special case where the Hessian is approximated via the Empirical Fisher approximation $\hat{F} = \frac{1}{m} \sum_{i=1}^m g_i g_i^T$, where the gradients $g_t \triangleq \nabla_\theta L(\theta_t)$ are stored in the matrix G , defined above. The first idea is to use the classic Woodbury-Sherman-Morrison (WSM) formula to integrate new gradient information as rank-1 updates into the current inverse. This leads to the following recursion to compute the IVHPs with an arbitrary vector $x \in \mathbb{R}^d$:

$$\hat{F}_{t+1}^{-1} x = \left(\hat{F}_t + \frac{1}{m} g_t g_t^T \right)^{-1} x \stackrel{(WSM)}{=} \hat{F}_t^{-1} x - \frac{\hat{F}_t^{-1} g_t (\hat{F}_t^{-1} g_t)^T}{m + g_t^T \hat{F}_t^{-1} g_t} x = \frac{1}{\lambda} x - \sum_{k=1}^t \frac{\hat{F}_k^{-1} g_k (\hat{F}_k^{-1} g_k)^T}{m + g_k^T \hat{F}_k^{-1} g_k} x \quad (4)$$

where $F_0 = \lambda I_d$ and $\lambda > 0$ is a damping parameter. The key technical idea behind M-FAC is the authors' observation that IHVPs can be expressed as a linear combination between the past gradients in the sliding window, where the coefficients are efficiently computed based only on scalar products $g_i^T g_j$ and $g_i^T x$, leading to the following expression for the IHVPs:

$$\hat{F}_m^{-1} x = \frac{1}{\lambda} x - \sum_{k=1}^m c_k g_k \quad (5)$$

This idea allows M-FAC to efficiently add or remove gradients from the sliding window: this is done by computing the corresponding coefficients c_k , and then making the resulting update into the formula for $\hat{F}_m^{-1} x$. Since M-FAC gives a FIM approximation based on empirical Fisher, it is implicitly a trust region method. The dampening parameter λ is inversely proportional to the unknown trust region radius R and it controls the behavior of the optimizer. When λ is small M-FAC is similar to Newton's method, while large λ reduces to SGD with a scaled learning rate η_t/λ .

Another important aspect to take into account for this method is regularization. Recent work [44] explains that weight decay and L_2 -regularization coincide for SGD, but are different for preconditioned gradient methods. We emphasize

that inputting $g_t = \nabla_{\theta} L(\theta) + \gamma\theta$ into the M-FAC preconditioner invalidates the empirical Fisher definition due to the additional term $\gamma\theta$. Based on this, and differently from the original M-FAC implementation [12], we decouple the regularization and use the update $\theta_{t+1} = (1 - \gamma)\theta_t - \eta_t \hat{F}_t^{-1} \nabla_{\theta} L(\theta_t)$, where γ is the weight decay parameter.

The GGT method can be seen as the full-matrix version of AdaGrad optimizer. Given the gradient history matrix $G \in \mathbb{R}^{d \times m}$ defined above, storing the last m gradients, GGT preconditions the last gradient as follows:

$$\theta_{t+1} = \theta_t - \eta_t \left[(GG^T)^{1/2} + \epsilon I_{d \times d} \right]^{-1} \nabla_{\theta} L(\theta_t) \quad (6)$$

Since working with the full GG^T matrix is infeasible, the authors use the singular value decomposition $G = U\Sigma V^T$ to derive a rank- m update for the preconditioned gradient $g_t \triangleq \nabla_{\theta} L(\theta_t)$ based on the following expression: $[(GG^T)^{1/2} + \epsilon I]^{-1} g = \frac{1}{\epsilon} g + U_m \left[(\Sigma_m + \epsilon I_m)^{-1} - \frac{1}{\epsilon} I_m \right] U_m^T g$, where $U_m \in \mathbb{R}^{d \times m}$ is the matrix containing the first m eigenvectors and $\Sigma_m \in \mathbb{R}^{m \times m}$ is the top-left block of the matrix $\Sigma \in \mathbb{R}^{d \times m}$ containing the m singular values. The matrix U_m can be efficiently computed by using the eigenvalue decomposition $G^T G = V \Sigma_m^2 V^T$ and then $U_m = GV \sqrt{\Sigma_m^+}$, where A^+ is the Moore-Penrose pseudo-inverse of matrix A .

Other Methods. Obtaining efficient approximations of second-order (curvature) information in deep learning is an active area. The *diagonal* approximation of the Hessian [19, 18] is very popular; however, it is known to provide lower quality relative to both block-wise methods or K-FAC [40, 35]. K-FAC provides a block diagonal approximation of the FIM, and allows efficient computation of the inverse [6, 31, 43, 40, 21]; however, it is known that its prerequisites do not always hold [28]. *Hessian-free* optimization [26] forgoes the explicit computation of Hessians in favor of computing an IHVP, but may require several iterations to converge. AdaHessian [42] provided an alternative approximation of the inverse Hessian diagonal, using Hutchinson’s randomized algorithm for estimating the diagonal, which requires smoothing heuristics, and has at least 2x iteration cost vs SGD. Shampoo [15] provides an efficient alternative to GGT, reducing memory cost by maintaining preconditioner estimates per model tensor, using an efficient iterative method to compute preconditioner inverses.

The Error Feedback Mechanism. The error feedback mechanism has been studied extensively in the context of gradient compression for standard SGD, in the absence of complex preconditioning. The first analyses of sparsified SGD with error feedback were provided by [36, 3] under additional assumptions, while [17, 37, 29] provided significant additions to the analysis.

3 Method

We now describe a generic algorithm for compressing gradient history required by the GGT and M-FAC algorithms, and then discuss how leverage this idea to drastically reduce memory cost via sparsification (Section 3.1) or low-rank compression (Section 3.2).

Algorithm 1 EFPC: Error Feedback for Compressed Full-Matrix Preconditioners

```

1: Parameters  $T$  (number of steps) and  $m$  (gradient history)                                ▷ optimization parameters
2:  $\xi_0 = 0_d \in \mathbb{R}^d$                                                                     ▷ initialize error
3: for each step  $t \in \{1, 2, \dots, T\}$  do
4:    $g_t \leftarrow \nabla_{\theta} L(\theta_t)$                                                         ▷ obtain gradient
5:    $a_t \leftarrow \xi_{t-1} + g_t$                                                             ▷ add gradient to previous error
6:    $c_t \leftarrow \text{COMPRESS}(a_t)$                                                         ▷ compress the accumulator using either sparsity or low-rank
7:    $\xi_t \leftarrow a_t - c_t$                                                                 ▷ update error
8:    $u_t \leftarrow \mathcal{A}(c_t)$                                                             ▷ update  $G$  and precondition using  $\mathcal{A}$ 
9:    $\theta_{t+1} \leftarrow \theta_t - \eta_t u_t$                                                   ▷ parameter update;  $\eta_t$  is an optional learning rate
10: end for

```

Overview. The general approach is described in Algorithm 1. Conceptually, we wish to only feed *compressed* gradients into the preconditioner estimate C_t , maintained by generic algorithm \mathcal{A} in our pseudo-code. Doing so directly, e.g. via direct gradient compression, leads to divergence (see Section 4). Instead, we employ a variant of *error feedback* [34, 9, 3, 17], using an error accumulator vector $\xi_t \in \mathbb{R}^d$, initially zero. At each step t , we accumulate the new gradient g_t and the previous error ξ_{t-1} into an accumulator a_t , which is compressed using our method of choice. The compressed accumulator c_t is then used to update the error buffer ξ_t and to update the sliding window G in the optimization procedure \mathcal{A} , to generate the descent direction u_t . Updating G means replacing the oldest compressed accumulator c_{t-m} with the latest c_t . Note that the actual representation of c_t may differ, depending on the compression method used.

The Diagonal Case. In the *diagonal case*, described in detail in Appendix Algorithm 5, our algorithm is justified theoretically. Specifically, we can adapt a recent argument by [24] to show that the method should guarantee standard rates of $O(1/\sqrt{T} + \sigma^2/\sqrt{T} + d/T)$ under standard assumptions on the objective, that is 1) Smoothness; 2) Unbiased and bounded stochastic gradients; and 3) Bounded variance. Specifically, obtaining this result requires specializing the constants corresponding to AMSGrad, in the preconditions to their Corollary 1. In future work, we plan to investigate provable convergence in the full-matrix case.

3.1 Compressing Preconditioners via Sparsity and Error Feedback

We now detail accumulator compression via sparsity, specifically by using Top- k sparsification and error feedback. Specifically, the preconditioner data structure will only store $k \ll d$ entries from each accumulated gradient, where k is around 1% of the full dimension d . In turn, this can essentially remove the memory overhead of full-matrix preconditioning. We detail our approach for the Sparse GGT algorithm; the Sparse M-FAC variant is similar and will only be described in brief.

Sparse GGT. At a high level, we wish to leverage sparsity in the logical gradient history matrix $G \in \mathbb{R}^{m \times d}$. For this, we store it in the COOrdinate list sparse format, which requires storing matrix $\mathcal{V} \in \mathbb{R}^{m \times k}$ for values, matrix $\mathcal{R} \in \mathbb{Z}^{m \times k}$ for rows and $\mathcal{C} \in \mathbb{Z}^{m \times k}$ for columns. All these matrices can be stored in vector format, with dimension $m \cdot k$. This will be compatible with standard sparse operations, such as the Sparse Matrix-Matrix (SPMM) method in the PyTorch Sparse library [11].

We will use the tuple $(\mathcal{R}, \mathcal{C}, \mathcal{V})$ to refer to the sparse buffer G . We distinguish between \mathcal{V} , which is the internal state of the sparse buffer (holding the k most significant values from a_t) and \mathcal{V}_t , which is the output of Top- k operator at a single step. *With slight abuse of notation, we call the compressed accumulator $c_t = (\mathcal{V}_t, \mathcal{I}_t)$ a sparse gradient, even though it is an accumulation of gradients.* The matrix \mathcal{C} is created in such a way that each row contains the index of that row (e.g. $[0, \dots, 0; 1, \dots, 1; \dots; m-1, \dots, m-1]$) and is represented as a single vector where the rows are concatenated. Let $i \in \{0, \dots, m-1\}$ be an index indicating the location where the new gradient will be placed in the buffer $(\mathcal{R}, \mathcal{C}, \mathcal{V})$. At each step, we receive the accumulator a_t , the most significant k values \mathcal{V}_t and their corresponding indices \mathcal{I}_t . The expression $a_t[\mathcal{I}_t] \in \mathbb{R}^d$ will represent a “densified” version of a sparse vector, which contains zeros at indices $j \notin \mathcal{I}_t$.

We integrate the values and indices in the internal buffers \mathcal{V} and \mathcal{I} in row i using the indices α and β . Since the sparse $G \in \mathbb{R}^{m \times k}$ and we have to compute the scalar product $\delta = G^T x$, we can easily transpose the sparse G by swapping the rows and columns in the SPMM call. The scalar products matrix $G^T G$ is updated by overwriting the i^{th} row and column by δ . At this point we can perform eigenvalue decomposition of $G^T G$ and finally compute the update direction u_t by preconditioning the sparse accumulator $a_t[\mathcal{I}_t]$. The full procedure is presented in Algorithm 2.

Algorithm 2 Detailed Sparse GGT Implementation

```

1: Variables:  $\mathcal{V} \leftarrow 0 \in \mathbb{R}^{mk}$ ,  $\mathcal{R} \leftarrow 0 \in \mathbb{Z}^{mk}$ ,  $i \leftarrow 0$ ,  $G^T G \leftarrow 0 \in \mathbb{R}^{m \times m}$ 
2: Operators:  $\mathcal{C} \leftarrow \text{vec}([r \cdot 1_k]_{r=0}^{m-1}) \in \mathbb{Z}^{mk}$ 
3: procedure SPARSEGGT-STEP( $t, a_t \in \mathbb{R}^d, \mathcal{V}_t \in \mathbb{R}^k, \mathcal{I}_t \in \mathbb{Z}^k$ )
4:    $\alpha \leftarrow i \cdot k$ ,  $\beta \leftarrow \alpha + k$ ,  $\mathcal{V}_{\alpha:\beta} \leftarrow \mathcal{V}_t$ ,  $\mathcal{R}_{\alpha:\beta} \leftarrow \mathcal{I}_t$  ▷ integrate values and indices
5:    $\delta \leftarrow \text{SPMM}(\text{Sparse}(r = \mathcal{C}, c = \mathcal{R}, v = \mathcal{V}), \text{Dense}(a_t[\mathcal{I}_t]))$  ▷ compute  $G^T a_t[\mathcal{I}_t]$ 
6:    $\text{row}_i(G^T G) \leftarrow \delta$ ,  $\text{col}_i(G^T G) \leftarrow \delta$  ▷ update dot products in row and col  $i$ 
7:    $G^T G \leftarrow V \Sigma_m^2 V^T$ ,  $i \leftarrow (i + 1) \bmod m$  ▷ eigenvalue decomposition & index update
8:    $U_m \leftarrow \text{SPMM}(\text{Sparse}(r = \mathcal{R}, c = \mathcal{C}, v = \mathcal{V}), \text{Dense}(V \sqrt{\Sigma_m^{-1}}))$ 
9:    $u_t \leftarrow \frac{1}{\epsilon} (a_t[\mathcal{I}_t]) + U_m [(\Sigma_m + \epsilon I_m)^{-1} - \frac{1}{\epsilon} I_m] U_m^T (a_t[\mathcal{I}_t])$  ▷ compute GGT direction
10:  return  $u_t$ 
11: end procedure

```

Sparse M-FAC. We take a similar approach to sparsifying the M-FAC preconditioner. The gradient should be integrated into the circular history buffer. We then update the matrix $G^T G$ which holds the scalar products in M-FAC. We adopt a slightly different memory storage approach for the ring buffer G that allows us to compute the M-FAC IHVP. Recall that this is the difference between the vector to precondition and the linear combination of the sparse gradients in the buffer, following Equation 5. Concretely, we store two matrices, $\mathcal{V} \in \mathbb{R}^{m \times k}$ for values and $\mathcal{I} \in \mathbb{R}^{m \times k}$ for indices and two additional tensors, $r_m \in \mathbb{R}^m$ to store the scalar products that are computed in parallel and $r_d \in \mathbb{R}^d$ to accumulate the sparse gradients from the linear combination. Our sparse implementation does not interfere with the original CUDA kernels, which still achieve high efficiency. It is interesting to mention that even though the gradients used to build the preconditioner are $(d - k)$ -sparse, and the vector being preconditioned is sparse, the IHVPs are not. In fact, except for the initial warm-up period, IHVPs are usually dense.

Memory Savings. In general, the two optimizers have $\tilde{O}(mk)$ space complexity, where k is the target density of the gradients after Top- k compression. In practice, we obtain stable convergence for $k = d/100$, which translates into space savings of approximately 20x (relative to GGT) and 30x (relative to M-FAC). We detail the savings calculation and provide precise examples in the Appendix.

3.2 Compressing Preconditioners via Low-Rank Approximation and Error Feedback

In this section, we discuss an alternative approach for compressed preconditioners, via low-rank compression of the gradients. Specifically, we will implement the COMPRESS step in Algorithm 1 via a low-rank approximation of the gradient, using an efficient variant of power iteration [38]. Then, we consider the M-FAC algorithm, and reformulate its operations to leverage low-rank matrix operations for memory savings. We start by describing how the algorithm works a single layer, and then present the global algorithm, which computes preconditioning for the whole model.

Low-Rank M-FAC for a Single Layer. Assume that the gradient at a given layer of the model is represented by the s -dimensional tensor $g \in \mathbb{R}^{p_1 \times p_2 \times \dots \times p_s}$. To compress the tensor, we use a variant of power iteration [38] by firstly unfolding the tensor into a matrix $\tilde{g} \in \mathbb{R}^{p_1 \times p_{2:s}}$, where $p_{2:s} = \prod_{i=2}^s p_i$. This matrix is then iteratively multiplied by a rank ρ matrix $Q \in \mathbb{R}^{p_{2:s} \times \rho}$, which is reused from the previous iteration, to obtain the left decomposition matrix $P \in \mathbb{R}^{p_1 \times \rho}$. After orthogonalization of P , the updated right matrix Q is obtained from the relation $\tilde{g} = PQ^T$. Notice that P and Q have $(p_1 + p_{2:s})\rho$ elements which can be significantly smaller than $p_1 \cdot p_{2:s}$ for smaller ranks ρ . This compression procedure is outlined in Algorithm 3.

In order to “introduce” the current gradient g into the M-FAC preconditioner data structure, we firstly need to compute an inner product between previously stored gradients and g (see Equation 5). In matrix representation the product between two gradients corresponds to the Frobenius inner product. Specifically, for a given low-rank representation of gradient matrices $\tilde{g}_i = P_i Q_i^T$ and $\tilde{g}_j = P_j Q_j^T$, the Frobenius product can be written as $\text{Tr}(\tilde{g}_i^T \tilde{g}_j) = \text{Tr}(Q_i P_i^T P_j Q_j^T) = \text{Tr}((P_j^T P_i)^T (Q_j^T Q_i))$. Notice that matrix products $P_j^T P_i$ and $Q_j^T Q_i$ are only of size ρ by ρ , so we compute them explicitly and then perform summation over their element-wise products to get the final result. As full gradients do not appear in this expression, we store just left and right gradients P_i and Q_i and update the M-FAC inner product matrix as needed.

The final preconditioned gradient update is computed as a weighted sum of previous gradients. The weights are computed via dynamic programming on top of the inner product values as in the original M-FAC. The final weighted sum of gradients is obtained by sequentially adding gradients reconstructed from their low-rank representation $g_i = P_j Q_j^T$.

Algorithm 3 Power iteration compression algorithm [38]

```

1: procedure POWERCOMPRESS(gradient tensor  $g$ , previous  $Q$ ) ▷ applied for each layer
2:    $\tilde{g} \leftarrow g.\text{RESHAPE}(p_1, p_{2:s})$ 
3:    $P \leftarrow \tilde{g}Q$ 
4:    $P \leftarrow \text{ORTHOAGONALIZE}(P)$ 
5:    $Q \leftarrow \tilde{g}^T P$ 
6:   return  $(P, Q)$ 
7: end procedure

```

Global Low-Rank M-FAC. To obtain an equivalent algorithm to the original M-FAC, independent per-layer steps are not sufficient as we would lose cross-layer correlation information. Instead, we use linearity of the inner product to compute the final result efficiently. In the original version of M-FAC, a current complete gradient from a L -layered model is represented as a concatenation of flattened per-layer gradients $\hat{g} = (\hat{g}^1 \ \hat{g}^2 \ \dots \ \hat{g}^L)^T$, where \hat{g}^i is the gradient from layer i . In this, representation an inner product between two gradients \hat{g}_i and \hat{g}_j can be expressed in a block form as $(\hat{g}_i, \hat{g}_j) = \sum_{\ell=1}^L (\hat{g}_i^\ell, \hat{g}_j^\ell)$. This dot product is then used to update the inner product matrix $G^T G$.

In the context of our efficient scheme for single-layer low-rank update, we replace each inner product block by its low-rank counterpart to obtain the equivalent values. Recall that the computation of summation weights in the M-FAC needs access only to these inner products, so this part of the algorithm remains the same. The final gradient update is computed per-layer and we rely on linearity of the sum again to share the summation weights and dampening coefficient ϵ between layers. For more details refer to the pseudocode in Algorithm 4.

Memory Savings. At each layer, all m gradients of size $p_1 p_{2:s}$ in the ring buffer are replaced by a low-rank representation with $\rho(p_1 + p_{2:s})$ elements. For simplicity, assume the rank to be a small constant (e.g. 4 is a valid value in our experiments). If we assume that the $p_{2:s}$ term dominates in the sum, then the relative gain in memory is proportional to $p_1 p_{2:s} / p_{2:s} = p_1$. Similarly for tensors with dominating first dimension, the gain will be proportional

Algorithm 4 Low Rank M-FAC preconditioning

```

1: INPUT: per-layer compressed  $((P^1, Q^1), \dots, (P^L, Q^L))$  gradients
2: STATE: per-layer ring buffers  $G^\ell$  with compressed gradient history; full inner products  $G^T G$ 
3: procedure LOW RANK M-FAC  $((P^1, Q^1), \dots, (P^L, Q^L))$ 
4:    $\delta \leftarrow$  zero vector of size  $m$  ▷ new full inner product
5:   for each layer  $\ell \in \{1, 2, \dots, L\}$  do ▷ aggregate inner products across the whole model
6:     Update  $G^\ell$  with current gradient  $(P^\ell, Q^\ell)$ 
7:     for each time step  $\tau \in \{t - m + 1, \dots, t\}$  do
8:        $\delta_{t-\tau} \leftarrow$  low-rank inner product  $\text{Tr}((g_\tau^\ell)^T (P^\ell (Q^\ell)^T))$ 
9:     end for
10:  end for
11:  Update row and column in  $G^T G$  from  $\delta$ 
12:  M-FAC: compute summation weights  $w \in \mathbb{R}^m$  from  $G^T G$ 
13:  for each layer  $\ell \in \{1, 2, \dots, L\}$  do
14:     $u_t^\ell \leftarrow \epsilon^{-1} P^\ell (Q^\ell)^T + \sum_{\tau=t-m+1}^t w_\tau g_\tau$  ▷ aggregate gradients from the ring buffer
15:  end for
16:  return vector of per-layer updates  $u_t$ 
17: end procedure

```

to the size of the rest of the tensor. For example, for the BERT-tiny model, Full M-FAC requires at least 18 GBs of memory, whereas Rank-1 M-FAC, which recovers accuracy, consumes less than 2 GB, achieving a 9x-improvement. We provide concrete examples in Table 10.

4 Experiments

We now use compressed implementations for GGT and M-FAC in various settings, using small and medium-scale CV and NLP models. Our purpose is to show that sparse and low-rank implementations recover the accuracy of their dense counterparts at a smaller memory cost. For the sparse approach we use $k = 1\%$ gradient density and rank 1 to 8 in the compression schema in algorithm 1 and $m_{GGT} = 100$ and $m_{MFAC} = 1024$ for all experiments. We use notation μ for momentum, η for the initial learning rate, γ for weight decay, λ for M-FAC dampening, k for gradient density, ρ for rank, E for epochs, γ_η for learning rate decay, B for batch size.

Linear Probing. We begin by examining a simple yet practical problem, that of linear probing over accurate pre-trained features. Specifically, we create a dataset of 1.2 million 768-dimensional features, taken by extracting outputs from the final convolutional layer of a CLIP-trained [32] 4x-rescaled ResNet-50 model, for which we wish to perform linear probing on ImageNet-1K [33]. We therefore train a multi-class logistic regression on the ImageNet dataset for 10 epochs, using different optimization algorithms, such as GD, SGD, full & batch L-BFGS and dense (D) & sparse (S) GGT and M-FAC. Table 1 summarizes our results in terms of both loss and validation accuracy on ImageNet. We use standard values $m = 100$ for GGT and $m = 1024$ for MFAC; full parameters are given in the Appendix.

Table 1: Results for Linear Probing on ResNet50/ImageNet. The first row describes the optimization algorithm (**F**=full, **B**=batch, **S**=sparse, **D**=dense); the 2nd training loss; 3rd shows test accuracy.

GD	SGD	F-LBFGS	B-LBFGS	D-GGT	S-GGT	D-MFAC	S-MFAC
1.4790	0.7141	0.7738	0.4588	0.3790	0.3679	0.3406	0.4751
69.40%	78.79%	77.20%	80.54%	80.81%	80.69%	80.25%	81.40%

We observe that full-matrix preconditioners (GGT and M-FAC) both obtain competitive results with standard parameter values, relative to SGD, GD, and full-batch (F) or batched (B) L-BFGS. Focusing on the effects of sparsity, we observe that S-GGT obtains lower training loss and slightly lower test accuracy relative to the dense version. S-MFAC is able to generalize better compared to D-MFAC, despite its higher training loss. Since the problem is convex, all dense optimizers should reach the optimum by exhaustively tuning the hyper-parameters. We can view the competitive performance of the compressed optimizers as encouraging.

MNIST/MLP. To compare with other preconditioners, we integrated S-MFAC with the recently-introduced ASDL preconditioning framework [30]. Thus, we compare against several other approaches, such as AdamW [25], PSGD [23], K-FAC [27], K-BFGS [13], SENG [41], and Shampoo [15]. Table 2 shows validation accuracy results on the standard

Table 2: The test-set accuracy of **S-MFAC** in the ASDL library [30] benchmark on the MLP ($w=2048$) model and MNIST dataset.

SGD	AdamW	PSGD (KF)	K-BFGS	K-FAC	SENG	Shampoo	S-MFAC
99.2	99.1	99.2	99.0	99.2	99.1	99.2	99.2

MNIST ASDL benchmark for an MLP of width 2048, where each method has been tuned independently following the protocol of ASDL [30]. Sparse M-FAC with 1% density matches the top accuracy of all other methods.

Computer Vision Experiments. Our next experimental setup covers ResNet-20 [16] ($d = 0.27M$) for CIFAR-10 [20] and ResNet-18 ($d = 11.7M$) for ImageNet [7]. For the latter, we follow the FFCV [22] recipe, removing image resizing. We train models from scratch using SGD with momentum, dense and sparse GGT (99% sparsity) and M-FAC and low-rank M-FAC (rank 4). We decouple the weight decay γ from the gradient, and apply it in the optimizer, which allows us to compare the loss values.

Table 3: Results for ResNet-20 on CIFAR10. The first row reports the training loss and second row validation accuracy. The number in parentheses indicate stdev (for training loss, this is within 0.001).

	SGD	D-MFAC	S-MFAC	D-GGT	S-GGT	LR-MFAC
Loss	0.032	0.017	0.017	0.108	0.097	0.021
Acc.	92.16 (.10)	92.12 (.13)	92.25 (.21)	87.77 (.22)	87.73 (.34)	91.43 (.30)

CIFAR-10/ResNet-20. The results in Table 3 show validation accuracy on the ResNet20/CIFAR-10 experiment. We observe that 1) Dense(D) M-FAC reaches similar accuracy to SGD, whereas Dense(D) GGT achieves lower accuracy in this task; 2) Sparse(S) M-FAC reaches the same accuracy as the dense variant (and SGD); 3) Low-Rank(LR) M-FAC with rank 4 reaches $< 0.8\%$ lower accuracy relative to the best results.

CIFAR-10/ResNet-18 We integrate S/D-MFAC into the ASDL framework [30] that has a few particular settings which are important to mention. First, the preconditioned gradient is automatically clipped to have fixed norm before updating the model parameters. Secondly, the batch-normalization (BN) layers outside the residual blocks of the model are ignored from the optimization (only the running statistics are updated during training, but not the learnable parameters), while the BN layers inside the model blocks are inputted to the optimizer along with the parameters in the convolutional and fully-connected layers.

We observed that clipping influences the results of our optimizer and because of that we experiment with this feature on and off. In addition, we set up three different scenarios for the parameters in the BN layers: 1) ignore *all* from optimization (do not include any BN parameters in the optimizer at all), 2) ignore *none* (include all parameters in BN layers in the optimizer) and 3) ignore the BN modules (include only the BN layers in the residual blocks of the model, thus recovering the standard ASDL setup).

ASDL scales the preconditioned gradient to norm 10 and performs grid search for the learning rates. We adopt the same approach by using the learning rates reported by the authors and perform grid search for dampening λ .

In table 6 we present our results for scenario 1 where we optimize all weights of the model (including BN) and *without clipping*. We used $E \in \{20, 100\}$ and $B \in \{32, 128\}$ for 3 and 5 seeds. Since we do not scale the preconditioned gradient to a specific norm, we found that learning rate $\eta = 10^{-3}$ (the smallest value in the original grid) performed the best among all. We choose λ using a grid, which is described in table 5. In table 6 we report the test accuracy for the runs that scored the highest validation accuracy (as in the original ASDL paper), as well as their corresponding training loss, validation and test accuracy plots in figures 8, 9, 10, 11, 12, 13.

We explore the influence of optimizing the parameters in the BN layers. For this experiment we adopt the three scenarios as *ignore none*, *ignore all*, *ignore modules* along with the options of clipping the preconditioned gradient to norm 10 or not performing the clipping at all, resulting 6 scenarios in total. We use the learning rates $\eta = 0.03$ when we apply clipping and $\eta = 10^{-3}$ when we do not apply clipping (both these values can be found in the ASDL grid search sets). We present the results of this ablation study in the table 4. For each particular BN scenario, clipping yields lower validation and test accuracy in general because the scaling of the preconditioned gradient in S-MFAC is larger, thus showing that clipping hurts the accuracy of our optimizer. The BN scenario S_3 proposed by the original ASDL paper yields the highest test accuracy among all three scenarios that we tested on.

Table 4: Ablation study on BN parameters for CIFAR-18 on RN-18 using S-MFAC with $k = 1\%$, $E = 20$, $B = 32$, $\gamma = 5e - 4$. Clipping value *yes* stands for rescaling the preconditioned gradient to norm 10. The abbreviation S_n stands for scenario n . We report mean accuracy over three runs with seeds 1, 2, 3.

BN scenario	clipping	val accuracy	test accuracy	hyper-params
optimize all (S_1)	no	92.64 ± 0.16	91.87 ± 0.07	$\eta = 1e - 3, \lambda = 5e - 7$
	yes	92.00 ± 0.29	91.07 ± 0.05	$\eta = 3e - 2, \lambda = 5e - 5$
ignore all (S_2)	no	92.03 ± 0.40	91.38 ± 0.19	$\eta = 1e - 3, \lambda = 5e - 7$
	yes	91.79 ± 0.20	91.00 ± 0.16	$\eta = 3e - 2, \lambda = 1e - 6$
ignore modules (S_2)	no	92.73 ± 0.35	92.02 ± 0.13	$\eta = 1e - 3, \lambda = 1e - 7$
	yes	91.99 ± 0.24	91.27 ± 0.05	$\eta = 3e - 2, \lambda = 5e - 7$

Table 5: Search grid for S/D-MFAC on ASDL. s stands for *seed*.

E=20, B=32, S-MFAC	$s \in [5], \lambda \in \{i \cdot 10^{-5}, i \cdot 10^{-6} \mid \forall i \in [9]\}$
E=20, B=128, D-MFAC	$s \in [5], \lambda \in \{i \cdot 10^{-5}, i \cdot 10^{-6} \mid \forall i \in [9]\}$
E=100, B=128, S-MFAC	$s \in [3], \lambda \in \{10^{-7}, 5 \cdot 10^{-7}, 10^{-6}, 3 \cdot 10^{-6}, 5 \cdot 10^{-6}, 7 \cdot 10^{-6}, 8 \cdot 10^{-6}, 10^{-5}, 5 \cdot 10^{-5}\}$
E=100, B=128, D-MFAC	$s \in [3], \lambda \in \{10^{-7}, 5 \cdot 10^{-7}, 10^{-6}, 3 \cdot 10^{-6}, 5 \cdot 10^{-6}, 7 \cdot 10^{-6}, 8 \cdot 10^{-6}, 10^{-5}, 5 \cdot 10^{-5}\}$

Table 6: Final hyper-parameters for S/D-MFAC on ASDL. We use $\eta = 1e - 3, \mu = 0, \gamma = 5e - 4$

Scenario	Hyper-parameters	Train Loss	Val Acc (%)	Test Acc (%)
E=20, BS=32, S-MFAC	$\lambda = 5e - 7$	0.8246 ± 0.07	92.65 ± 0.35	91.94 ± 0.20
E=20, BS=128, D-MFAC	$\lambda = 1e - 6$	0.7967 ± 0.07	92.47 ± 0.39	92.09 ± 0.50
E=100, BS=128, S-MFAC	$\lambda = 7e - 6$	0.6147 ± 0.01	96.27 ± 0.15	95.71 ± 0.15
E=100, BS=128, D-MFAC	$\lambda = 1e - 5$	0.6302 ± 0.03	95.97 ± 0.50	95.41 ± 0.07

CIFAR-10/ViT-Tiny For these settings we also use ASDL framework and only test S-MFAC. Based on the experiment on ResNet-18, we adopt the scenario 3 for the layer normalization (LN) layers (e.g. the modules are ignored from optimizer, but the parameters in LN layers in the blocks are included in the optimizer). We use 3 seeds to perform grid search over the values mentioned in the ASDL paper and we experiment with the clipping feature on and off. We present our results in table 7. Moreover, we restate the ASDL results in our paper and add our results for a better comparison in table 8.

Table 7: Ablation study on LN layers of ViT-Tiny for CIFAR-18 using S-MFAC with $k = 1\%$, $E = 20$, $B = 32$, $\gamma = 1e - 4$. Clipping value *yes* stands for rescaling the preconditioned gradient to norm 10.

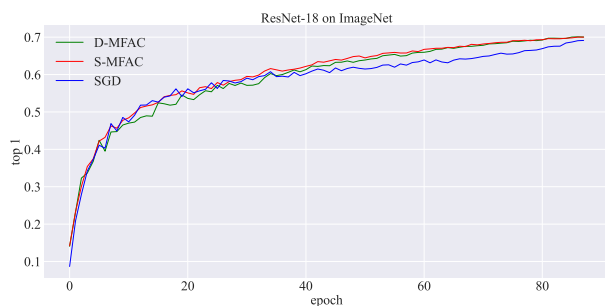
LN status	clipping	val accuracy	test accuracy	hyper-params
ignore modules	no	97.65 ± 0.24	97.50 ± 0.07	$\eta = 1e - 3, \lambda = 5e - 5$
	yes	97.80 ± 0.21	97.76 ± 0.03	$\eta = 1e - 2, \lambda = 5e - 6$

ImageNet/ResNet-18. Next, we train ResNet-18 on ImageNet [7] using a highly-tuned version of SGD (with momentum) from the FFCV [22] library, as well as S/D-MFAC. All hyper-parameters are provided in the Appendix. Figure 1 shows the validation accuracy curves for this experiment. (The loss curves show similar trends, and are provided in the Appendix.) SGD obtains training loss 2.237 with accuracy 69.12%. D-MFAC reaches 2.164 loss and higher accuracy, 70.03%. Despite slightly higher training loss than D-MFAC (2.185), S-MFAC has comparable 70.01% validation accuracy. Thus, compressing the preconditioner recovers the accuracy of the dense optimizer. We ran the experiments on a single A100 GPU and recorded the GPU memory usage of the entire process via NVIDIA-SMI tool. SGD uses 14.5 GB and S-MFAC 15 GB, while D-MFAC needs 59 GB. In Figure 1 we examine the behavior of S-MFAC as we decrease gradient density on ResNet-18/ImageNet-1K. We observe that S-MFAC with $k = 0.17\%$ ($\approx 20k$ weights) still achieves comparable accuracy to SGD, and that accuracy decreases very gradually.

Table 8: Original ASDL test accuracy augmented with our S-MFAC results with clipping to norm 10 and BN/LN scenario 3 (ignore only the BN/LN modules and optimize the ones in the blocks). For RN-18, we only show the results for 20 epochs.

Method	MNIST/MLP(w=2048)	CIFAR-10/RN18	CIFAR-10/viT-T
SGD	99.2	91.2	97.8
AdamW	99.1	89.9	97.9
PSGD (KF)	99.2	93.3	98.0
K-BFGS	99.0	91.4	97.7
K-FAC (1mc)	99.2	93.6	97.4
SENG	99.1	91.6	97.7
Shampoo	99.2	92.5	98.0
S-MFAC	99.2	92.02	97.76

Figure 1: Left: validation (Top-1) accuracy for ResNet18 training from scratch on ImageNet-1K. M-FAC and 99%-Sparse M-FAC reach approximately 1% higher validation accuracy relative to SGD using the well-tuned FFCV recipe [22]. Right: ablation study over gradient density k on ResNet-18 on ImageNet-1K. For a better comparison, top row shows D-MFAC and the bottom row shows SGD.



Density k	Train Loss	Test Accuracy
D-MFAC (100%)	2.164	70.03%
117k (1.00%)	2.185	70.01%
100k (0.85%)	2.183	70.18%
75k (0.64%)	2.187	69.99%
50k (0.42%)	2.190	69.68%
25k (0.21%)	2.206	69.43%
20k (0.17%)	2.217	69.26%
15k (0.12%)	2.230	69.05%
10k (0.08%)	2.246	68.84%
5k (0.04%)	2.300	68.27%
SGD	2.237	69.12%

Language Models. Finally, we tested our implementations for BERT models (TINY, MINI and BASE versions) on the SQUADv2 and MNLI task from the GLUE benchmark [39], comparing against the Adam optimizer with default settings from Hugging Face. Dense M-FAC with a window size of 1024 can only run on TINY and MINI models, requiring 19 GB and 45 GB memory, respectively, and runs out of memory (OOM) for the BASE model. The results in Table 9 show that our sparse implementation not only recovers the performance on these two models, but also allows us to run on BERT-base, with superior validation accuracy relative to Adam using standard hyper-parameters.

Table 9: Our results for BERT **T**iny, **M**ini and **B**ase. For GLUE-MNLI we report evaluation accuracy and for QA-SquadV2 we report the F1-score. OOM stands for Out of Memory error.

	Adam			S-MFAC			D-MFAC		
	T	M	B	T	M	B	T	M	B
MNLI	66.86	74.77	84.80	70.85	76.40	84.81	69.26	76.39	OOM
SQv2	49.94	57.87	75.73	52.22	60.70	76.37	52.44	61.08	OOM

5 Memory Usage & Running Time

We provide some additional details related to memory usage reported by NVIDIA-SMI and the total training time for the tasks described above. We note that the reported training time fluctuates depending on the machine load and therefore we report the minimum running time among all seeds. Table 10 summarizes our results.

Table 10: Final hyper-parameters for S/D-MFAC on ASDL. OOM stands for Out Of Memory.

Dataset	Model	Optimizer	Memory	Training Time	Comments
ImageNet	ResNet-18	SGD	14.49 GB	5h 45m	1x RTX-3090
		D-MFAC	58.87 GB	14h	1x A-100
		S-MFAC	14.95 GB	8h 45m	1x RTX-3090
CIFAR-10	ResNet-20	SGD	2 GB	35m	1x A-6000
		D-MFAC	3.1 GB	40m	1x A-6000
		S-MFAC	2.6 GB	1h	1x A-6000
CIFAR-10	ResNet-18	D-MFAC	46 GB	3h 50m	ASDL ($B = 128$)
		S-MFAC	4.9 GB	6h 19m	ASDL ($B = 128$)
GLUE/MNLI	BERT-Tiny	Adam	1.46 GB	14m	1x A-6000
		S-MFAC	2.54 GB	1h 10m	1x A-6000
		D-MFAC	18.82 GB	1h 20m	1x A-6000
	BERT-Mini	Adam	1.92 GB	21m	1x A-6000
		S-MFAC	3.59 GB	2h 31m	1x A-6000
		D-MFAC	45.87 GB	3h 25m	1x A-6000
	BERT-Small	Adam	2.62 GB	33m	1x A-6000
		S-MFAC	6.84 GB	1h 30m	1x A-6000
		D-MFAC	-	-	OOM
	BERT-Medium	Adam	3.50 GB	56m	1x A-6000
		S-MFAC	9.57 GB	2h	1x A-6000
		D-MFAC	-	-	OOM
	BERT-Base	Adam	6.27 GB	1h 56m	1x A-6000
		S-MFAC	22.12 GB	4h 47m	1x A-6000
		D-MFAC	-	-	OOM

6 Preconditioning Quantification

In this section we look at two metrics to quantify how well the preconditioned SGD works compared to raw SGD. Specifically, we are interested in how the preconditioned gradient $u = C^{-1}g$ aligns with the raw gradient g . This is motivated by the fact that it is impossible to explicitly have access to the preconditioning matrix C^{-1} to analyze it at each step (using eigenvalue decomposition, for example). In GGT and Dense/Sparse-MFAC we do not explicitly compute the curvature matrix, but directly compute u instead. Preconditioning has the effect of rotating and scaling the gradient g and in the next two subsections we are discussing two metrics which are able to quantify these two changes in g .

6.1 Rotation

To quantify the rotation, we simply compute the cosine similarity between g and u . In the context of M-FAC, we can get an SGD-like behavior by increasing the dampening parameter λ and in this case M-FAC won't rotate the gradient. Our hyper-parameter tuning process is not only guided by the standard performance metrics such as training loss and test/validation accuracies, but we also aim to find a dampening value λ that achieves a cosine similarity smaller than 1. Computing cosine similarity is cheap and can be performed at each step without affecting the training performance.

6.2 Scaling

To quantify scaling we propose a technique that requires slightly more computational effort. First, we can compute the norm ratio $r = \frac{\|u\|_2}{\|g\|_2}$ in order to check how larger the preconditioned gradient u is compared to stochastic gradient g . However, this might not be indicative enough for whether the preconditioning works. For example, a large r might imply that a single component is scaled by a lot, while the others are just perturbed by a low-magnitude noise.

A more comprehensive approach is to create an empirical distribution \mathcal{R} using the quantities $r_i = \left| \frac{u_i}{g_i} \right|$, which record the scaling at each component level in absolute value because we are only interested in the scaling magnitude (not the sign). We can now check different statistics of the empirical distribution \mathcal{R} , such as quantiles 25, 50 and 75 to quantify the overall scaling of g . It is important to emphasize that the scale of values in the empirical distribution \mathcal{R} is directly

dependent to the learning rate η and the dampening λ and it is extremely difficult to state the relationship between these three quantities.

6.3 Examples

To demonstrate the effectiveness of these two metrics, we compute them for SGD and S/D-MFAC on ResNet-18/ImageNet settings. We re-implemented SGD to work with full-size tensors in order to be able to compute the two metrics. In appendix F we show the plots for the two metrics for each optimizer separately.

The average cosine similarity for D-MFAC is around 0.85, for S-MFAC is around 0.25 and for SGD with momentum is around 0.45 almost during entire training. We hypothesize that S-MFAC induces the largest rotation among all optimizers because the gradient goes through a series of transformations in algorithm 1 that each induces a rotation: adding error feedback to g to obtain the accumulator (step 5), compressing the accumulator (step 6) and preconditioning (step 8).

To quantify scaling, we look at quantiles q_{25}, q_{50}, q_{75} . For SGD, we have $q_{25} \approx 1$, $q_{50} \in [2, 2.5]$ and $q_{75} \in [4.5, 6]$, while for S-MFAC we have larger values: $q_{25} \in [50, 330]$, $q_{50} \in [100, 800]$ and $q_{75} \in [250, 2000]$ during the entire training. In table 11 we present some values for the quantiles for each optimizer at steps 50k, 100k, 150k and 200k (220k training steps in total). In table 12 we present the approximate values of the norm ratio $r = \|u\|_2/\|g\|_2$ (the overall norm ratio). We would like to point out that even though we used the linearly decaying learning rates, both M-FAC optimizers scale the update by a lot during the first half of the training.

Table 11: The quantile values for the empirical scaling distribution \mathcal{R} at specific steps.

Optimizer	Quantile	Step 50k	Step 100k	Step 150k	Step 200k
SGD	Q25	1	1	1	1.1
	Q50	2.4	2.4	2.4	2.5
	Q75	5.5	5.5	5.5	5.7
S-MFAC	Q25	235	340	180	120
	Q50	630	770	470	270
	Q75	1670	1870	1300	680
D-MFAC	Q25	9500	10800	7600	4700
	Q50	12500	13800	9900	5800
	Q75	16500	18500	12600	7400

Table 12: The approximate values for the norm ratio $r = \|u\|_2/\|g\|_2$ at specific steps.

Optimizer	Step 50k	Step 100k	Step 150k	Step 200k
SGD	2.3	2.3	2.3	2.4
S-MFAC	3350	450	3130	1770
D-MFAC	10700	12500	8700	5100

7 Discussion and Future Work

We have provided a versatile new tool for addressing the memory costs of adaptive full-matrix preconditioning, in the form of a series of methods which compress the gradient history, by leveraging an instance of the error feedback mechanism. We complement this mechanism via efficient sparse/low-rank algorithms for maintaining existing preconditioners, and have shown experimentally that our approach can essentially provide lossless compression when applied via sparsity, with remarkably large compression rates.

In future work, we plan to investigate theoretical justification for our method; while we provide a preliminary investigation for this in the Appendix, we note that obtaining general bounds appears challenging, as even in the case of standard SGD understanding error feedback required significant technical effort, e.g. [3, 17]. Another direction of future work is exploring larger-scale validation of our method for additional architectures and tasks, and for additional preconditioning mechanisms.

8 Acknowledgements

The authors thank Adrian Vladu, Alexandra Peste, Mher Safaryan and Elias Frantar for their valuable feedback, the IT department from Institute of Science and Technology Austria for the hardware support and Weights and Biases for the infrastructure to track all our experiments.

References

- [1] Naman Agarwal, Brian Bullins, Xinyi Chen, Elad Hazan, Karan Singh, Cyril Zhang, and Yi Zhang. Efficient full-matrix adaptive regularization. In *International Conference on Machine Learning*, pages 102–110. PMLR, 2019.
- [2] Naman Agarwal, Brian Bullins, and Elad Hazan. Second-order stochastic optimization for machine learning in linear time, 2016.
- [3] Dan Alistarh, Torsten Hoefler, Mikael Johansson, Nikola Konstantinov, Sarit Khirirat, and Cédric Renggli. The convergence of sparsified gradient methods. In *Advances in Neural Information Processing Systems*, pages 5973–5983, 2018.
- [4] S.-I. Amari. Natural gradient works efficiently in learning, 1998.
- [5] Shun-ichi Amari. Natural gradient works efficiently in learning. *Neural Computation*, 10(2):251–276, 1998.
- [6] Jimmy Ba, Roger Grosse, and James Martens. Distributed second-order optimization using kronecker-factored approximations. 2016.
- [7] Jia Deng, Wei Dong, Richard Socher, Li-Jia Li, Kai Li, and Li Fei-Fei. Imagenet: A large-scale hierarchical image database. In *2009 IEEE conference on computer vision and pattern recognition*, pages 248–255. Ieee, 2009.
- [8] Jacob Devlin, Ming-Wei Chang, Kenton Lee, and Kristina Toutanova. Bert: Pre-training of deep bidirectional transformers for language understanding, 2018.
- [9] Nikoli Dryden, Tim Moon, Sam Ade Jacobs, and Brian Van Essen. Communication quantization for data-parallel training of deep neural networks. In *2nd Workshop on Machine Learning in HPC Environments (MLHPC)*, pages 1–8, 2016.
- [10] John C. Duchi, Elad Hazan, and Yoram Singer. Adaptive subgradient methods for online learning and stochastic optimization. *J. Mach. Learn. Res.*, 12:2121–2159, 2010.
- [11] Matthias Fey et al. Pytorch-sparse library. https://github.com/rusty1s/pytorch_sparse.
- [12] Elias Frantar, Eldar Kurtic, and Dan Alistarh. M-fac: Efficient matrix-free approximations of second-order information, 2021.
- [13] Donald Goldfarb, Yi Ren, and Achraf Bahamou. Practical quasi-newton methods for training deep neural networks, 2021.
- [14] Roger Grosse and James Martens. A kronecker-factored approximate fisher matrix for convolution layers, 2016.
- [15] Vineet Gupta, Tomer Koren, and Yoram Singer. Shampoo: Preconditioned stochastic tensor optimization. In *International Conference on Machine Learning*, pages 1842–1850. PMLR, 2018.
- [16] Kaiming He, Xiangyu Zhang, Shaoqing Ren, and Jian Sun. Deep residual learning for image recognition, 2015.
- [17] Sai Praneeth Karimireddy, Quentin Rebjock, Sebastian U Stich, and Martin Jaggi. Error feedback fixes SignSGD and other gradient compression schemes. In *Proceedings of the Thirty-sixth International Conference on Machine Learning*, pages 3252–3261, 2019.
- [18] Diederik P. Kingma and Jimmy Ba. Adam: A method for stochastic optimization, 2014.
- [19] Shankar Krishnan, Ying Xiao, and Rif A Saurous. Neumann optimizer: A practical optimization algorithm for deep neural networks. *arXiv preprint arXiv:1712.03298*, 2017.
- [20] Alex Krizhevsky, Vinod Nair, and Geoffrey Hinton. Cifar-10 (canadian institute for advanced research).
- [21] César Laurent, Thomas George, Xavier Bouthillier, Nicolas Ballas, and Pascal Vincent. An evaluation of fisher approximations beyond kronecker factorization, 2018.
- [22] Guillaume Leclerc, Andrew Ilyas, Logan Engstrom, Sung Min Park, Hadi Salman, and Aleksander Madry. FFCV: Accelerating training by removing data bottlenecks. <https://github.com/libffcv/ffcv/>, 2022.
- [23] Xi-Lin Li. Preconditioned stochastic gradient descent. *IEEE Transactions on Neural Networks and Learning Systems*, 29(5):1454–1466, may 2018.

- [24] Xiaoyun Li, Belhal Karimi, and Ping Li. On distributed adaptive optimization with gradient compression. *arXiv preprint arXiv:2205.05632*, 2022.
- [25] Ilya Loshchilov and Frank Hutter. Decoupled weight decay regularization, 2019.
- [26] James Martens. Deep learning via hessian-free optimization. In *Proceedings of the 27th International Conference on International Conference on Machine Learning, ICML'10*, page 735–742, Madison, WI, USA, 2010. Omnipress.
- [27] James Martens, Jimmy Ba, and Matt Johnson. Kronecker-factored curvature approximations for recurrent neural networks. In *International Conference on Learning Representations*, 2018.
- [28] James Martens and Roger Grosse. Optimizing neural networks with kronecker-factored approximate curvature, 2015.
- [29] Giorgi Nadiradze, Ilia Markov, Bapi Chatterjee, Vyacheslav Kungurtsev, and Dan Alistarh. Elastic consistency: A general consistency model for distributed stochastic gradient descent. *arXiv preprint arXiv:2001.05918*, 2020.
- [30] Kazuki Osawa, Satoki Ishikawa, Rio Yokota, Shigang Li, and Torsten Hoefer. Asdl: A unified interface for gradient preconditioning in pytorch, 2023.
- [31] Kazuki Osawa, Yohei Tsuji, Yuichiro Ueno, Akira Naruse, Rio Yokota, and Satoshi Matsuoka. Large-scale distributed second-order optimization using kronecker-factored approximate curvature for deep convolutional neural networks. *2019 IEEE/CVF Conference on Computer Vision and Pattern Recognition (CVPR)*, Jun 2019.
- [32] Alec Radford, Jong Wook Kim, Chris Hallacy, A. Ramesh, Gabriel Goh, Sandhini Agarwal, Girish Sastry, Amanda Askell, Pamela Mishkin, Jack Clark, Gretchen Krueger, and Ilya Sutskever. Learning transferable visual models from natural language supervision. In *ICML*, 2021.
- [33] Olga Russakovsky, Jia Deng, Hao Su, Jonathan Krause, Sanjeev Satheesh, Sean Ma, Zhiheng Huang, Andrej Karpathy, Aditya Khosla, Michael Bernstein, et al. Imagenet large scale visual recognition challenge. *International Journal of Computer Vision*, 115(3):211–252, 2015.
- [34] Frank Seide, Hao Fu, Jasha Droppo, Gang Li, and Dong Yu. 1-bit stochastic gradient descent and its application to data-parallel distributed training of speech DNNs. In *Fifteenth Annual Conference of the International Speech Communication Association*, 2014.
- [35] Sidak Pal Singh and Dan Alistarh. Woodfisher: Efficient second-order approximation for neural network compression, 2020.
- [36] Sebastian U Stich, Jean-Baptiste Cordonnier, and Martin Jaggi. Sparsified sgd with memory. *Advances in Neural Information Processing Systems*, 31, 2018.
- [37] Sebastian U Stich and Sai Praneeth Karimireddy. The error-feedback framework: Better rates for sgd with delayed gradients and compressed communication. *arXiv preprint arXiv:1909.05350*, 2019.
- [38] Thijs Vogels, Sai Praneeth Karimireddy, and Martin Jaggi. PowerSGD: Practical Low-Rank Gradient Compression for Distributed Optimization. In *Advances in Neural Information Processing Systems*, volume 32. Curran Associates, Inc., 2019.
- [39] Alex Wang, Amanpreet Singh, Julian Michael, Felix Hill, Omer Levy, and Samuel R Bowman. GLUE: A multi-task benchmark and analysis platform for natural language understanding. In *Proceedings of the Seventh International Conference on Learning Representations*, 2019.
- [40] Chaoqi Wang, Roger Grosse, Sanja Fidler, and Guodong Zhang. Eigendamage: Structured pruning in the kronecker-factored eigenbasis, 2019.
- [41] Minghan Yang, Dong Xu, Zaiwen Wen, Mengyun Chen, and Pengxiang Xu. Sketchy empirical natural gradient methods for deep learning, 2021.
- [42] Zhewei Yao, Amir Gholami, Sheng Shen, Kurt Keutzer, and Michael W Mahoney. Adahessian: An adaptive second order optimizer for machine learning. *arXiv preprint arXiv:2006.00719*, 2020.
- [43] Wenyuan Zeng and Raquel Urtasun. MLPrune: Multi-layer pruning for automated neural network compression, 2019.
- [44] Guodong Zhang, Chaoqi Wang, Bowen Xu, and Roger Grosse. Three mechanisms of weight decay regularization, 2018.

Appendices

We restate the notations that we introduced at the beginning of section 4. We use notation μ for momentum, η for the initial learning rate, γ for weight decay, λ for M-FAC dampening, k for gradient density, ρ for rank, E for epochs, γ_η for learning rate decay, B for batch size.

A Logistic Regression / Synthetic training details

Our experimental setup for logistic regression on the synthetic dataset consists of a parameter search for each method, which we describe in the following tables (the bold values represent the final values that lead to the best results). We use $E = 10$, $B = 128$ and cosine annealing learning rate for all experiments (except GD and F-LBFGS where we use the entire dataset).

GD & SGD. We use $\mu = 0.9$, $\gamma = 0$ and perform a grid search over the η , presented in table 13. GD requires a large η because the dataset is large (1.2M images).

Table 13: Search grid for learning rate η for GD & SGD.

GD	$\eta \in \{2000, 2100, 2200, 2300, 2400, 2500, 2600, 2700, 2800, \mathbf{2900}\}$
SGD	$\eta \in \{0.1, 0.5, \mathbf{1}\}$

L-BFGS. We perform grid search for η for full and batch LBFGS, which are presented in table 14.

Table 14: Search grid for learning rate η for L-BFGS.

Full L-BFGS	$\eta \in \{0.1, \mathbf{1}, 2, 5, 10, 100\}$
Batch L-BFGS	$\eta \in \{0.0001, 0.001, 0.01, \mathbf{0.1}, 1\}$

D/S-MFAC. We use $m = 1024$, $k = 1\%$, $\mu = 0$, $\gamma = 0$ and perform grid search for η and λ , described in table 15. For both optimizers there were multiple pairs that reached the same performance and we state them separately in the table 15.

Table 15: Search grid for learning rate η and dampening λ for S/D-MFAC.

η, λ	1e-7, 1e-6, 1e-5, 1e-4, 1e-3, 1e-2, 1e-1, 1
η_D, λ_D	(1, 1e-2), (1e-1, 1e-3)
η_S, λ_S	(1, 1e-2), (1e-5, 1e-7), (1e-1, 1e-3), (1e-2, 1e-4), (1e-3, 1e-5), (1e-4, 1e-6)

D/S-GGT. We use window size $m = 100$, $k = 1\%$ and the grid in table 16. Again, we show the corresponding pairs (η, ϵ) for the best runs.

Table 16: Search grid for learning rate η and dampening ϵ for S/D-GGT.

η, ϵ	1e-7, 1e-6, 1e-5, 1e-4, 1e-3, 1e-2, 1e-1, 1
η_D, ϵ_D	(1, 1e-5)
η_S, ϵ_S	(1, 1e-5)

Training plots. In figures 2 and 3 we present the test accuracy and training loss for the logistic regression experiment and we intentionally omit GD from the plots for better visibility.

B RN-18 / ImageNet training details

In these experiments we use $E = 88$ and $B = 1024$. In particular, we set $\gamma = 1e-5$ for convolution and fully connected parameters and $\gamma = 0$ for batch-normalization parameters, thus fixing the issue in the main FFCV repository. We use linear learning rate decay for all three optimizers and disable image rescaling. We present the final hyper-parameters in table 17.

Table 17: Hyper-parameters for SGD and S/D-MFAC. We kept fixed $\gamma = 1e-5$.

SGD	$\eta = 0.5, \mu = 0.9$
D-MFAC	$\eta = 1e-3, \lambda = 1e-6, \mu = 0$
S-MFAC	$\eta = 1e-3, \lambda = 1e-7, \mu = 0$

C RN-20 / CIFAR-10 training details

In these experiments we use $E = 164$, $B = 128$ and decay the learning rate by a factor of $\gamma_\eta = 0.1$ at 50% and 75% of training. The final hyper-parameters for each method are summarized in table 18. The grid-search parameters are similar to table 15. We show training plots in figures 6 and 7.

Table 18: Final hyper-parameters

SGD	$\eta = 0.1, \mu = 0.9, \gamma = 5e-4$
D-GGT	$m = 100, \eta = 0.1, \epsilon = 1e-5, \gamma = 0$
S-GGT	$m = 100, \eta = 0.1, \epsilon = 1e-5, \gamma = 0$
D-MFAC	$m = 1024, \eta = 1e-3, \lambda = 1e-6, \mu = 0, \gamma = 1e-4$
S-MFAC	$k = 1\%, m = 1024, \eta = 1e-3, \lambda = 1e-4, \mu = 0, \gamma = 1e-4$
LR-MFAC	$\rho = 4, m = 1024, \eta = 1e-3, \lambda = 1e-6, \mu = 0, \gamma = 0$

D BERT training details

We use the HuggingFace repository and plug in our optimizers. We compare against default Adam baselines as follows. For GLUE/MNLI we use $E = 3, \eta = 2e-5, \gamma = 0$ and for SQuADv2 we use $E = 2, \eta = 3e-5, \gamma = 0$. D-MFAC uses the default parameters from the original paper, e.g. $\eta = 1e-4, \lambda = 1e-6, \gamma = 0$ and we adopt the same values for S-MFAC for BERT-TINY/MINI. For BERT-BASE we use $\lambda = 5e-5$ for S-MFAC.

E Ablation study of low rank decomposition

To determine how the size of the decomposition rank ρ affects the effectiveness of the low rank M-FAC algorithm, we perform a series of experiments on ResNet-20 and BERT models. For ResNet-20 we use CIFAR-10 dataset and the same parameters as in the main experiments. For BERT family we use TINY, MINI and BASE variants and evaluate them on MNLI task from GLUE benchmark. For both setups we vary the rank from 1 to 8 and report the final test accuracy in the Table 19.

We observe that the decomposition rank significantly affects smaller BERT models but barely influences BERT-BASE and RN-20 model results. While the exact reason for such behaviour is not obvious, we hypothesise that for RN-20 the decomposition is effective even at rank 1 due to gradient tensors already having a small first dimension, resulting in small compression error. We also note that Rank 8 BERT-BASE run diverged, requiring more investigation into the stability of the training.

F Quantifying Preconditioning

This section shows plots for the cosine similarity in figure 14, the norm ratio in figure 15 and the statistics of empirical distribution \mathcal{R} in figures 16, 17 and 18.

Table 19: Test accuracy on CIFAR-10 dataset for ResNet-20 (RN-20) and on MNLI for BERT-TINY, -MINI and -BASE, trained with Low-Rank M-FAC with different decomposition ranks ρ .

rank ρ	RN-20	TINY	MINI	BASE
1	91.40	57.34	66.88	84.42
2	91.19	63.49	68.76	84.44
4	91.43	66.44	70.93	84.45
8	91.13	67.90	72.22	—

Algorithm 5 Diagonal AdaGrad with Error Feedback

```

 $\xi_0 = 0_d \in \mathbb{R}^d$  ▷ initialize error
 $G_0 = 0_d \in \mathbb{R}^{d \times d}$  ▷ initialize diagonal
for each step  $t \in \{1, 2, \dots, T\}$  do
   $g_t \leftarrow \nabla_{\theta} L(\theta_t)$ 
   $a_t \leftarrow \xi_{t-1} + g_t$  ▷ add gradient to previous error
   $c_t \leftarrow \text{TOPK}(a_t)$  ▷ compress the accumulator
   $\xi_t \leftarrow a_t - c_t$  ▷ update the error
   $G_t \leftarrow G_{t-1} + \text{diag}(c_t^2)$  ▷ update diagonal
   $\theta_{t+1} \leftarrow \theta_t - \eta_t \text{diag}(G_t)^{-1/2} c_t$ 
end for

```

Figure 2: Epoch vs test accuracy

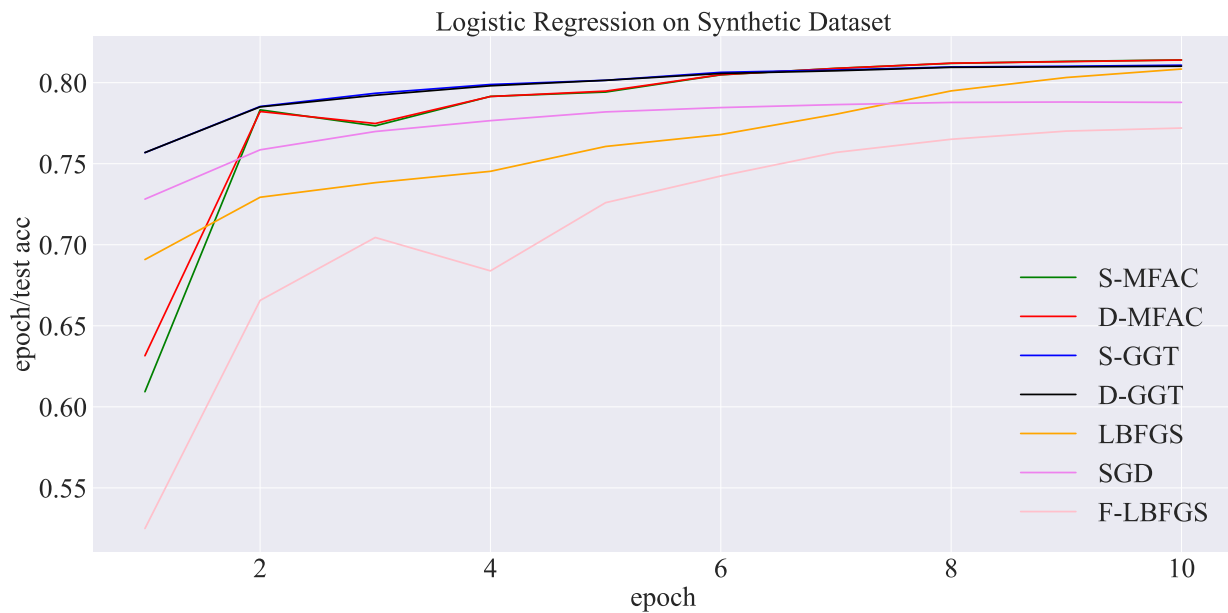


Figure 3: Epoch vs training loss

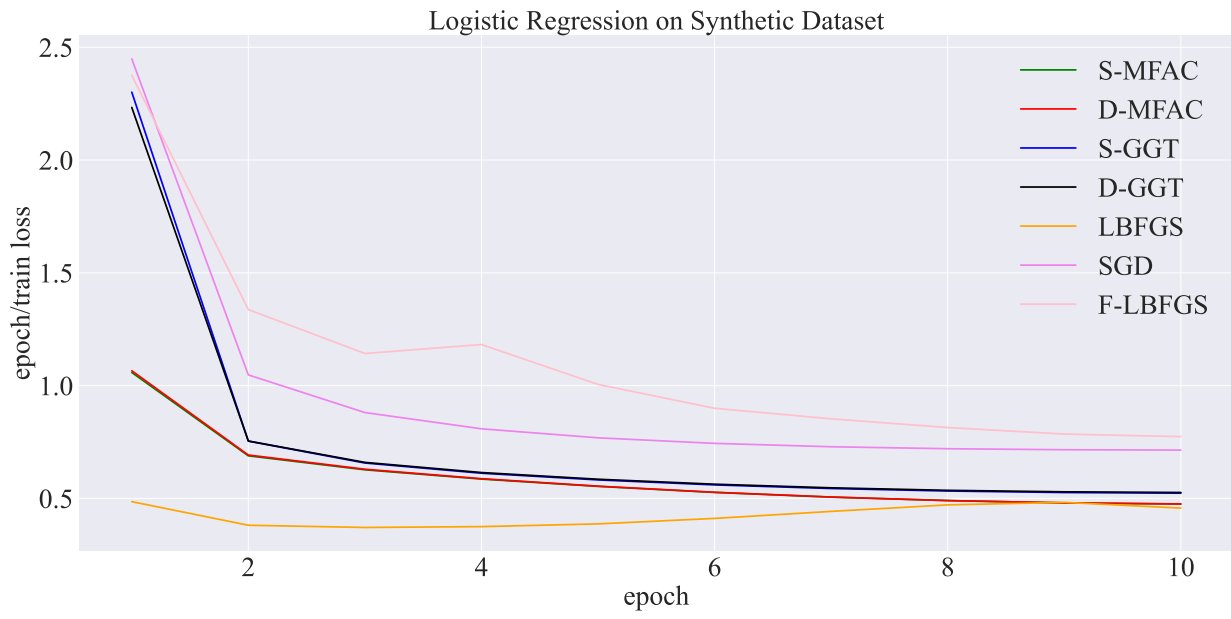


Figure 4: Epoch vs top-1 test accuracy for ResNet-18 on ImageNet

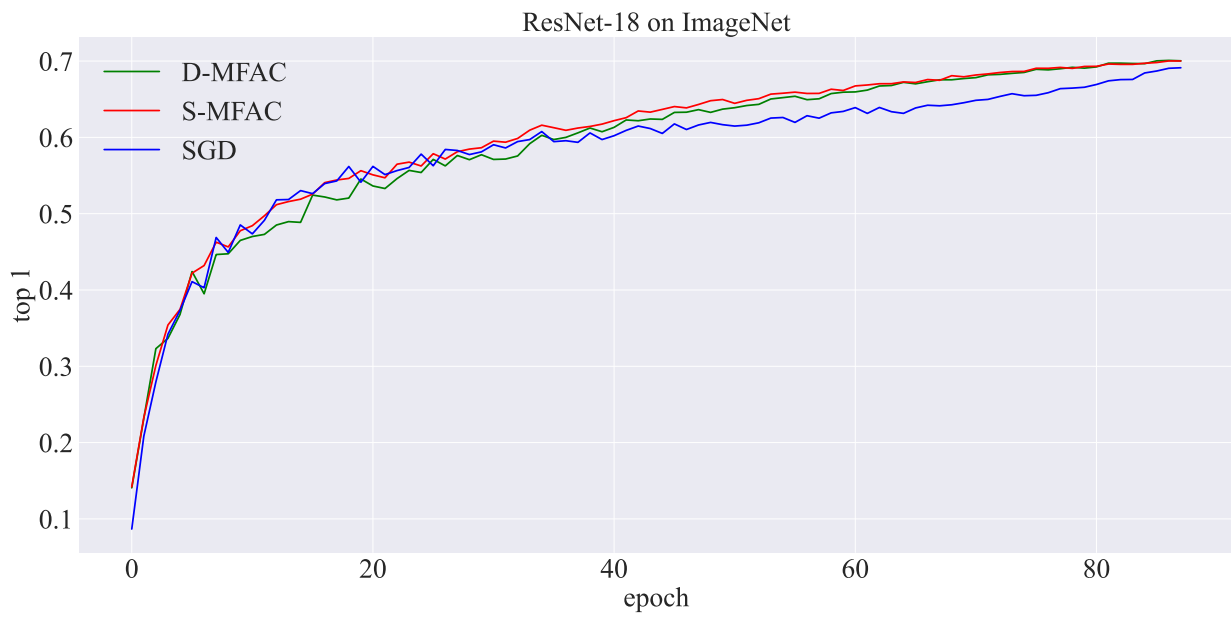


Figure 5: Epoch vs train accuracy for ResNet-18 on ImageNet

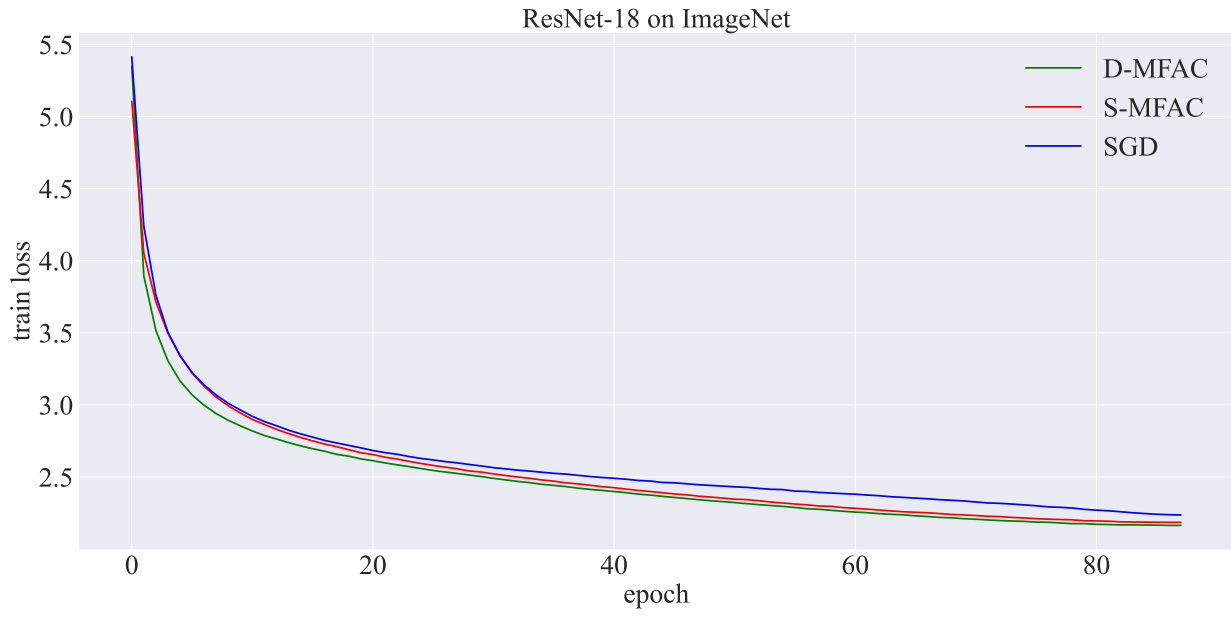


Figure 6: Epoch vs train loss for ResNet-20 on CIFAR-10

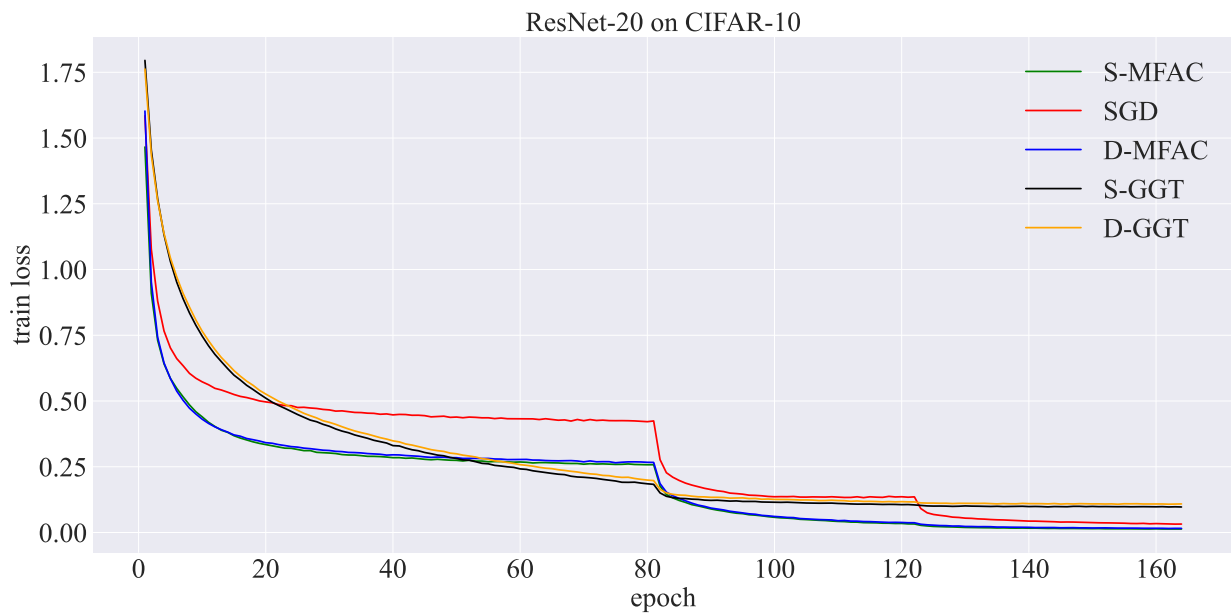


Figure 7: Epoch vs test accuracy for ResNet-20 on CIFAR-10 on ASDL

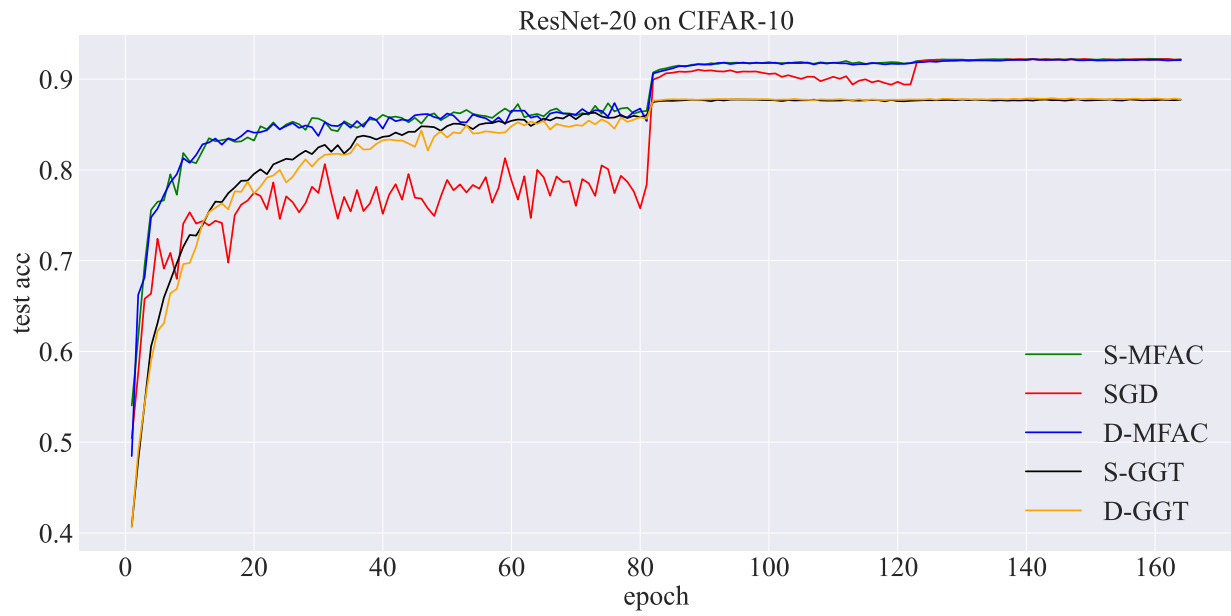


Figure 8: Epoch vs train loss for ResNet-18 on CIFAR-10

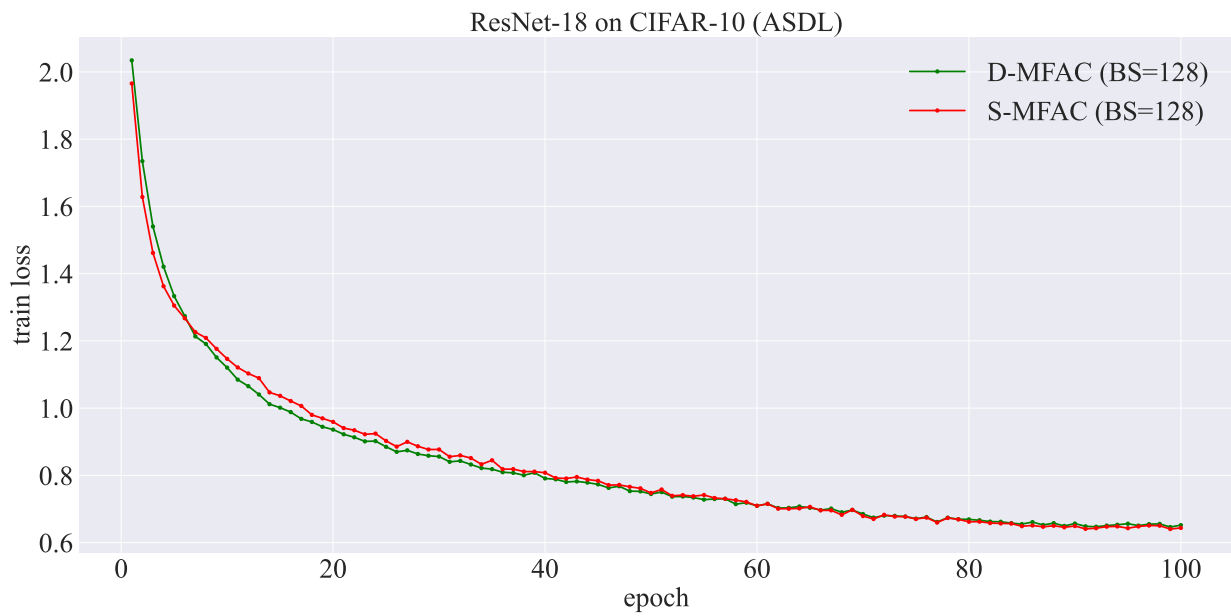


Figure 9: Epoch vs validation accuracy for ResNet-18 on CIFAR-10

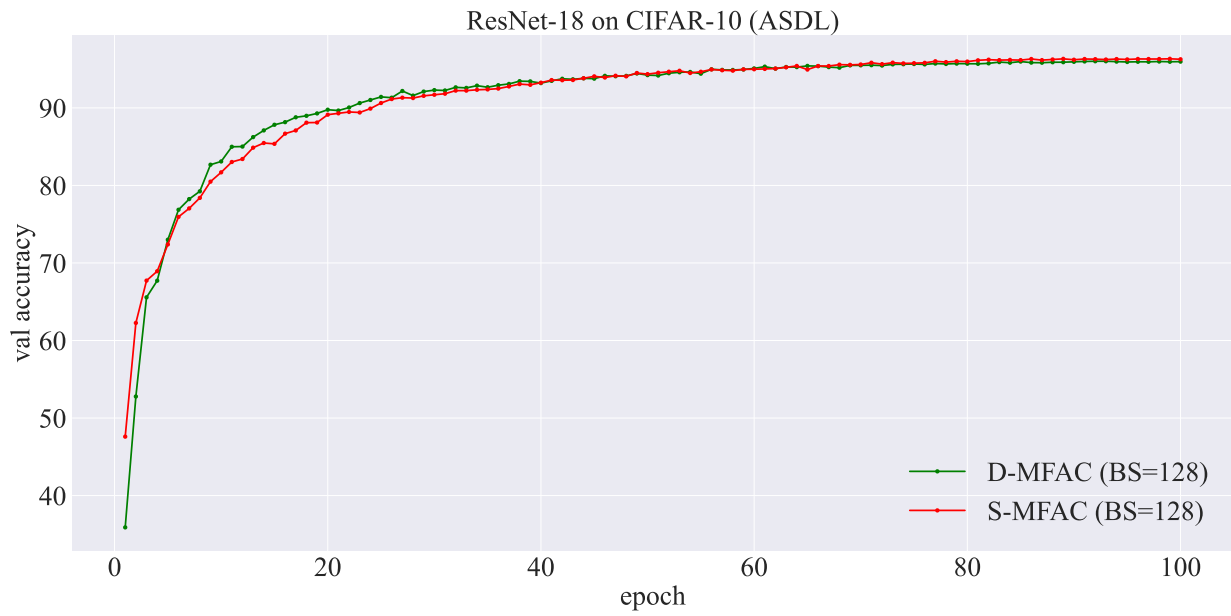


Figure 10: Epoch vs test accuracy for ResNet-18 on CIFAR-10 on ASDL

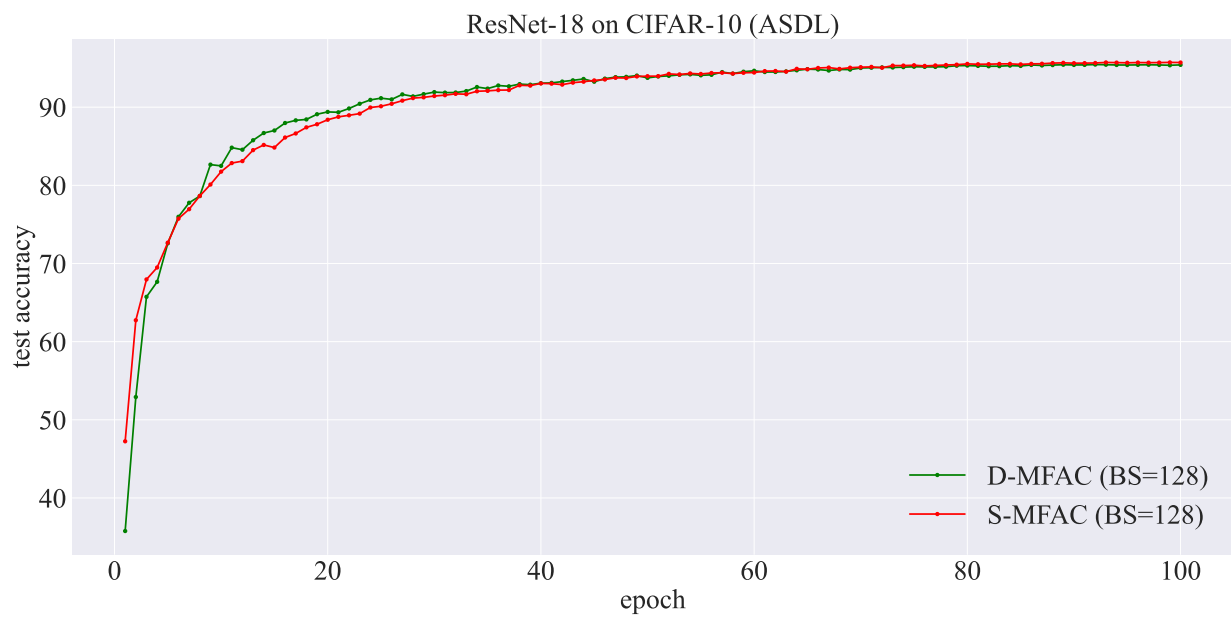


Figure 11: Epoch vs train loss for ResNet-18 on CIFAR-10

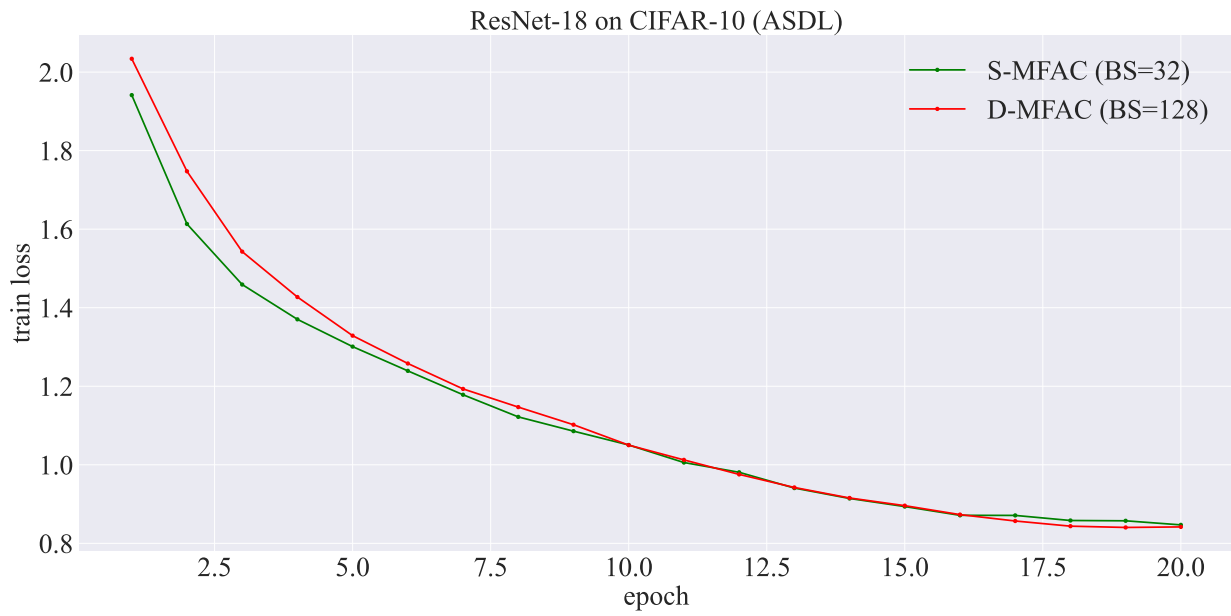


Figure 12: Epoch vs validation accuracy for ResNet-18 on CIFAR-10

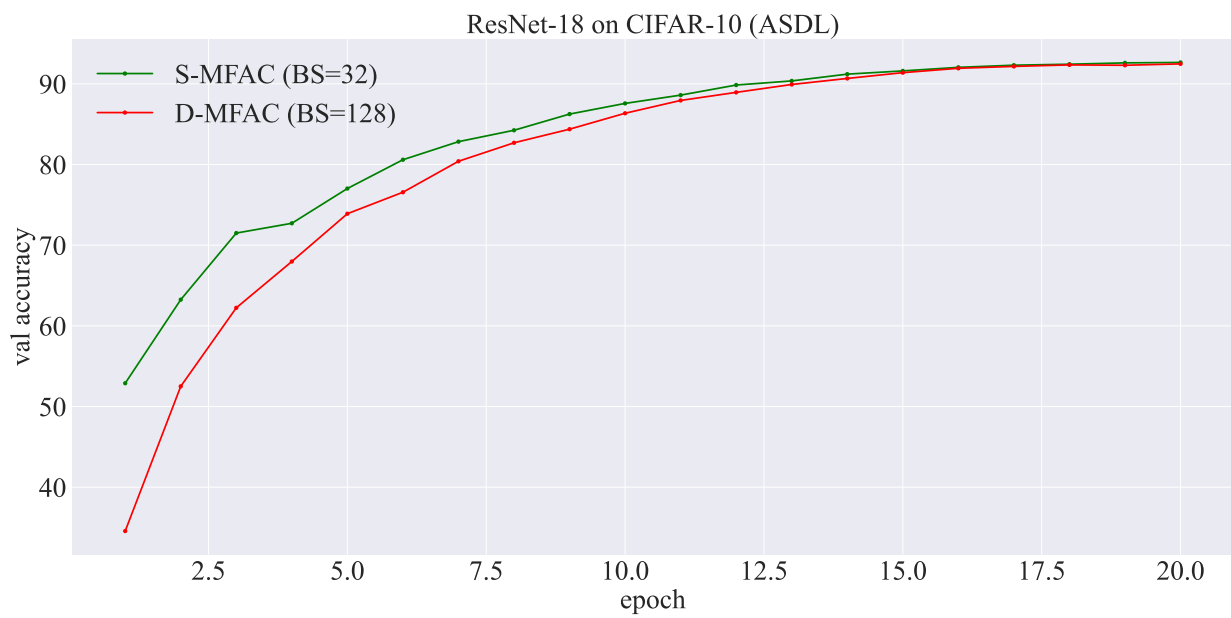


Figure 13: Epoch vs test accuracy for ResNet-18 on CIFAR-10 on ASDL

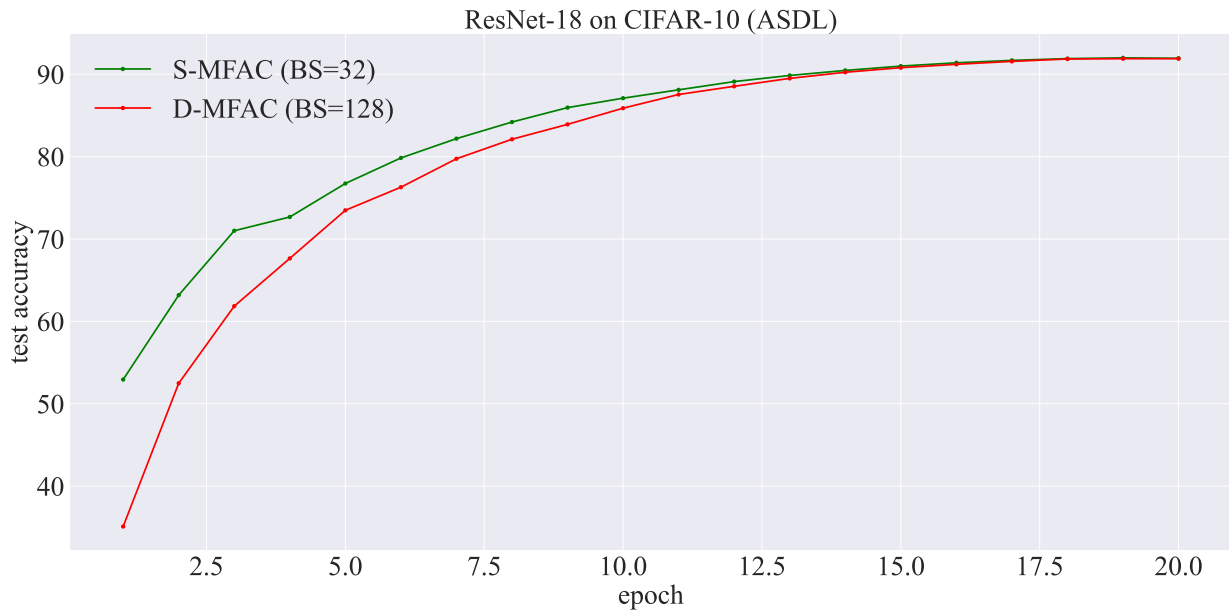


Figure 14: Rotation metric: cosine similarity between u and g . For SGD (green), u is the momentum accumulator.

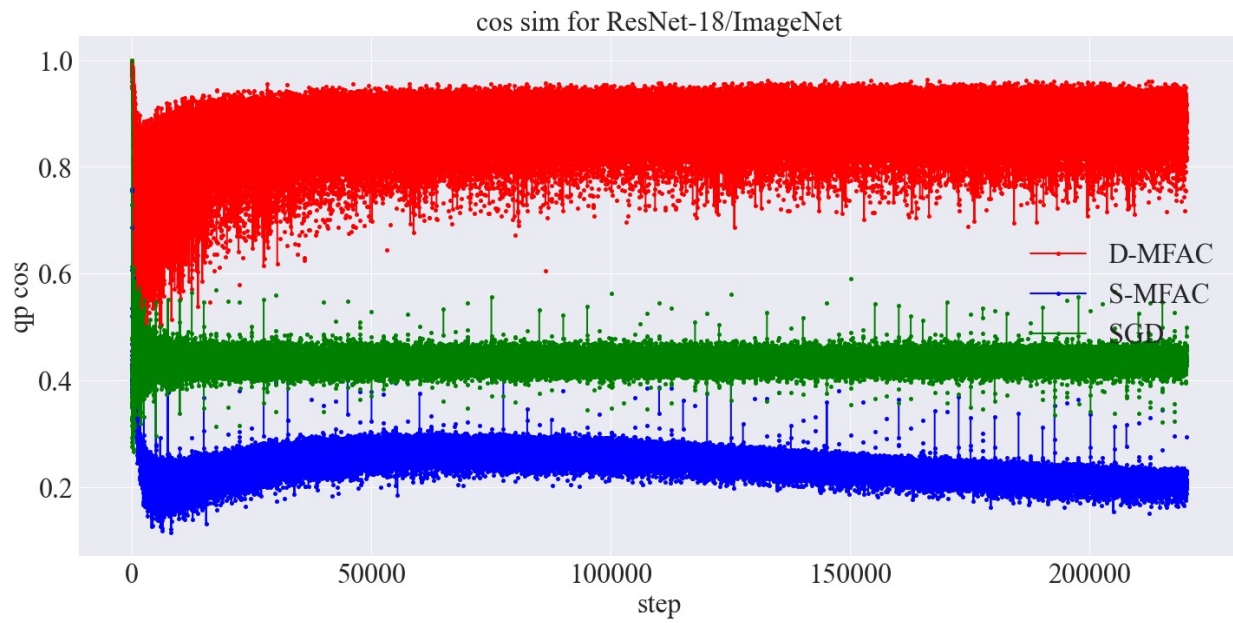


Figure 15: Scaling metric: norm ratio $r = \frac{\|u\|_2}{\|g\|_2}$. For SGD, the values are in interval $[2, 2.5]$.

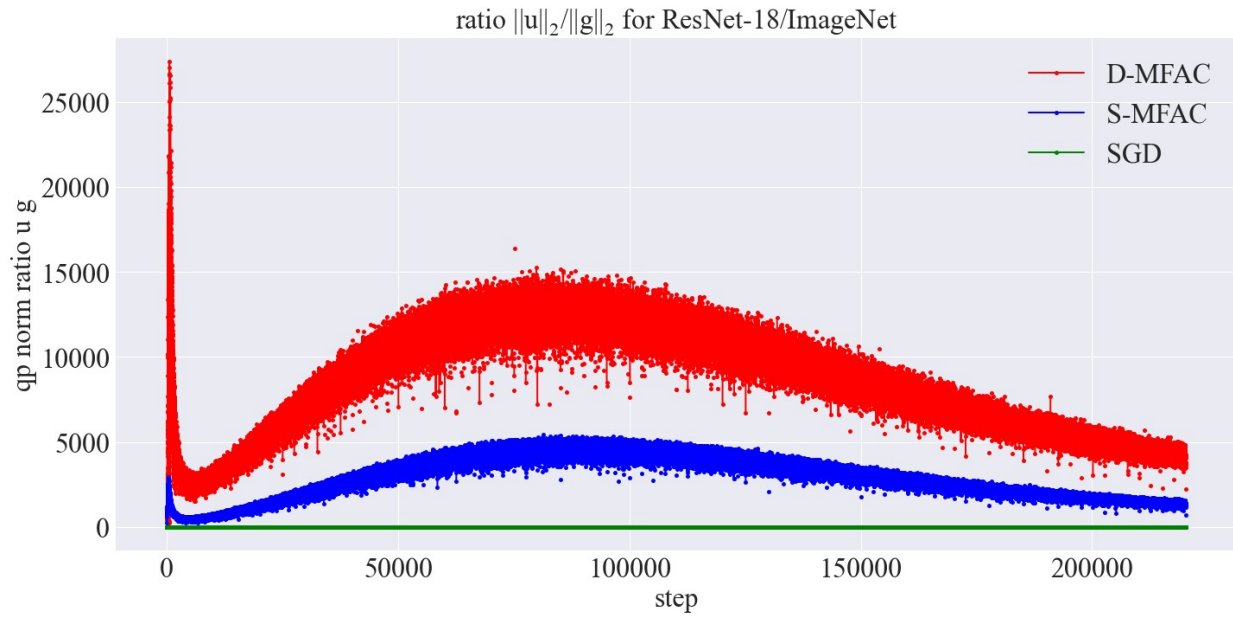


Figure 16: Scaling metric: Q25 for empirical distribution \mathcal{R} . For SGD, the values are around 1 and for S-MFAC are in interval $[50, 330]$

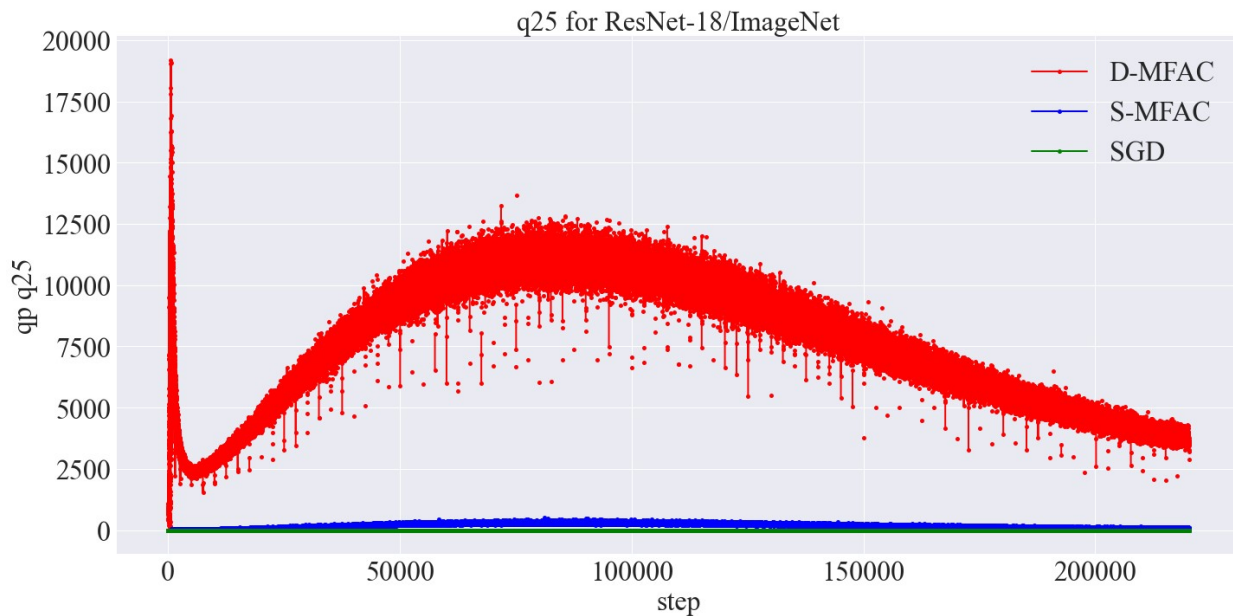


Figure 17: Scaling metric: Q50 for empirical distribution \mathcal{R} . Values for S-MFAC are in interval $[100, 800]$ and for SGD in interval $[2, 2.5]$

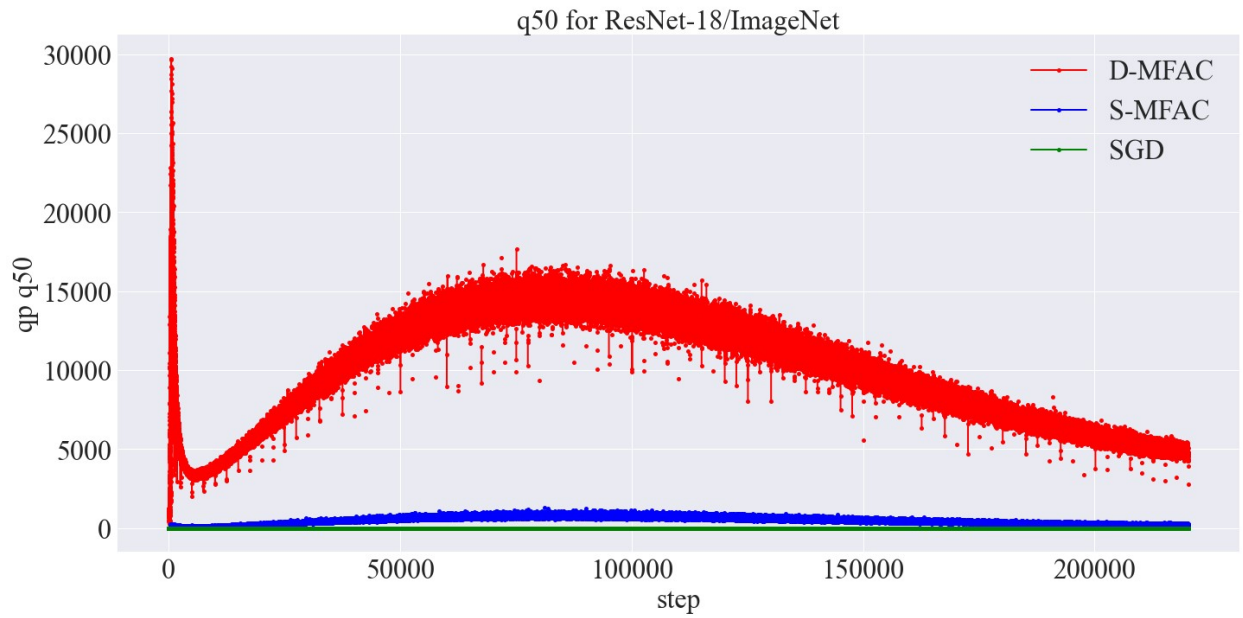


Figure 18: Scaling metric: Q75 for empirical distribution \mathcal{R} . Values for S-MFAC are in interval $[250, 2000]$ and for SGD in interval $[4.5, 6]$

